

Uniformization and Constructive Analytic Continuation of Taylor Series

Ovidiu Costin and Gerald V. Dunne

Department of Mathematics, The Ohio State University, Columbus, OH 43210-1174, USA

Department of Physics, University of Connecticut, Storrs, CT 06269-3046, USA

Abstract

We analyze the general mathematical problem of global reconstruction of a function with least possible errors, based on partial information such as n terms of a Taylor series at a point, say the origin, possibly also with coefficients of finite precision. We refer to this as the “inverse approximation theory” problem, because we seek to reconstruct a function from a given approximation, rather than constructing an approximation for a given function.

Within the class of functions analytic on a common Riemann surface Ω , bounded on Ω , or with the same rate of growth in the natural metric on Ω , and a common Maclaurin series, we prove an optimality result on their reconstruction at other points on Ω , and provide a method to attain it. The procedure uses the uniformization theorem, and the optimal reconstruction errors depend only on the distance to the origin.

We provide explicit uniformization maps for some Riemann surfaces Ω of interest in applications. Some of these can also be obtained as a rapidly convergent limit of compositions of elementary maps. One such map is the covering of $\mathbb{C} \setminus \mathbb{Z}$ by curves with fixed origin, modulo homotopies, precisely the one needed in the analysis of the Borel plane of the *tritronquée solutions* to the Painlevé equations P_I – P_V . As an application we show that this uniformization map leads to dramatic improvement in the extrapolation of the P_I *tritronquée* solution throughout its domain of analyticity and also into the pole sector.

Given further information about the function, such as is available for the ubiquitous class of resurgent functions, significantly better approximations are possible and we construct them. In particular, any chosen one of their singularities can be eliminated by specific linear operators which we introduce, and the local structure at the chosen singularity can be obtained in fine detail. These operators involve convolutions, whose singularity nature we analyze. More generally, for functions of reasonable complexity, based on the n th order truncates alone we propose new efficient tools which are convergent as $n \rightarrow \infty$, and which provide near-optimal approximations of functions globally, as well as in their most interesting regions, near singularities or natural boundaries.

1 Introduction

In problems of high complexity in mathematics and physics it is often the case that a solution can only be generated as a perturbation series at certain special points, usually with only a finite number of terms, and often also with coefficients known only with finite precision. Under these circumstances, we ask what is the optimal strategy to approximate the underlying function, and if optimality cannot be achieved in practice, what are the most efficient near-optimal methods? On a practical level, this question has been encountered in many problems in the literature, and

dealt with in various problem-specific ways [40, 8, 44, 74, 14, 16]. However, an underlying mathematical foundation and theory seems to be lacking. As a mathematical question this is related to, but distinct from, conventional approximation theory. We formulate this mathematical problem as a problem of *inverse approximation theory*: here the approximation is fixed, in the form of a number n of terms of a series, and the underlying function F is to be reconstructed as accurately as possible in the large n limit. In contrast to other methods (such as Padé approximants) our reconstruction methods may involve different operators for different points in the domain of analyticity, and can achieve rigorous *pointwise* convergence results rather than being limited to convergence in capacity. This flexibly adaptive approach is motivated by the following class of questions that we wish to address:

1. Where are the singularities of F ?
2. What is the nature of each singularity?
3. What is the local behavior or more generally what are the associated local expansions (in physics, fluctuation functions) near each singularity?
4. How far can one explore the full Riemann surface of F ?
5. Can one quantify the expected precision locally, especially near the singularities, as a function of how much input data (and of what precision) is given?

In physical applications, question 1 corresponds to identifying critical points or saddle points, which typically have important mathematical and physical implications (e.g. asymptotics and phase transitions). Question 2 refers to determining whether these singularities are algebraic or logarithmic branch points (or in special simple cases, poles), or essential singularities. An important application in statistical physics and quantum field theory is the accurate determination of critical exponents [74]. Questions 3 and 4 involve for example the numerical determination of Stokes constants, or wall-crossing formulas, or generally the fluctuations about a given critical point. Question 5 is of particular practical value, since in nontrivial problems it is often difficult to generate many terms of the original series. We ask how much information about the global structure of the underlying function can be decoded from a finite order expansion, generated at a particular location. Here we are motivated by the theory of resurgent functions, which are ubiquitous in analysis and in applications, and for which the general philosophy suggests that a considerable amount of global information is encoded in local expansions [37, 11, 20, 61, 51, 5]. For example, for resurgent functions information concerning not just the location of the singularities, but also their nature, is accessible by analytic and numerical means. We develop methods that can exploit this additional structure.

For resurgent functions, such as the tritronquée solutions of the Painlevé equations (see [39] and references therein), uniformization provides a practical way (and perhaps the only one that does not require full knowledge about the function) to access the higher Riemann sheets, needed in medianization and other forms of averaging. Écalle-Borel summation (the generalization of Borel summation that applies to functions with singularities along the axis of Laplace transform) crucially relies on such averaging [37, 56, 19].

The series may be convergent or factorially divergent, and in the latter case a Borel transform restores convergence. This is the case of asymptotic expansions in ordinary differential or difference equations near singularities of nontrivial Poincaré rank, or in similar settings in difference equations, in PDEs such as the Schrödinger equation at small or large times, and in parabolic PDEs for small times, among many examples.

Many *ad hoc* methods have been developed in different mathematical and physical contexts to address some of these problems [40, 8, 44, 74, 14, 16]. Here we develop a systematic mathematical approach. We also present new quantitative comparisons of some of the common methods, and some improvements of their implementation.

We begin with an optimality result, for which the construction can be made fully explicit in certain classes of problems with enough symmetry. This class includes the *tritronquée* solutions¹ of Painlevé equations P_I – P_V and can be used in the Painlevé project [62] to calculate these solutions with vastly improved accuracy over the existing methods, see §6.2. Theorem 1 constructs the best approximants (based on partial Maclaurin sums) to F in generic classes of functions analytic on a common Riemann surface and sharing a common bound. Optimality is achieved with a uniformization map, which also provides rigorous numerical access to the higher sheets of the Riemann surface. Theorem 1 also provides a benchmark with which to compare a variety of approximate methods for situations where optimality is impractical or impossible. Compared to existing techniques, the gain in accuracy is particularly dramatic near singular points.

We then address the problem of reconstructing a given function when an exact uniformization of the corresponding Riemann surface is not known, but when further information about the nature of the function’s singularities may be known, either analytically or approximately. For the wide class of resurgent functions, prevalent in applications, stronger results are obtained. In §4, §5 and §6 we develop a new set of practical approximation methods which can achieve near-optimal results, especially in the most interesting regions of the function’s underlying Riemann surface, near the singularities.

In Section 6.2 we give as an example the reconstruction with extreme precision of the P_I *tritronquée* solution from 200 terms of its asymptotic expansion (passing through a Borel transform to restore convergence) throughout its sector of analyticity, and also in the opposite pole sector where we find the first 66 poles to high precision. The accuracy dramatically improves over existing methods. Similar reconstructions can be applied to the other Painlevé *tritronquée* solutions. Such extreme precision has applications to the Painlevé project [62], and also to the spectral properties of certain Schrödinger operators [58, 60].

1.1 Settings, Notations, and Organization of the Paper

In the following, $\mathbb{D}_r(a)$ denotes the open disk of radius r , centered at a . The unit disk centered at the origin appears often in the discussion, and is simply denoted $\mathbb{D} = \mathbb{D}_1(0)$, with boundary the unit circle: $\mathbb{T} = \partial\mathbb{D}$. The Riemann sphere is written as $\hat{\mathbb{C}} = \mathbb{C} \cup \{\infty\}$.

We consider functions defined on Ω , a **simply connected Riemann surface**. An important special case in applications is Ω being a simply connected domain strictly contained in \mathbb{C} , so the uniformization map is its usual Riemann conformal map to \mathbb{D} .

Ω is assumed to contain \mathbb{D} **strictly**. More precisely, if Ω is uniformized to \mathbb{D} by ψ , then ψ is analytic in \mathbb{D} and $\psi(0) = 0$. In the special case when Ω is a covering of $\hat{\mathbb{C}} \setminus S$ where S is a discrete set, this means Ω is described by equivalence classes of curves **originating at zero, modulo homotopies in $\hat{\mathbb{C}} \setminus S$** .² We shall call such Riemann surfaces coverings with fixed origin.³

The set S may contain points in \mathbb{D} , meaning functions living on Ω might be singular at points in \mathbb{D} on higher sheets of Ω . By the uniformization theorem, Ω is biholomorphically equivalent

¹Solutions with asymptotic series expansions in the largest possible sector.

²Using $\hat{\mathbb{C}}$ is a standard convention, since it makes a counting difference for the analyzed functions if infinity is singular or not. For instance, $\ln[(1 - \omega)/(1 + \omega)]$ is analytic at infinity and its Riemann surface is uniformized on the plane, after a Möbius change of variable.

³The choice of a fixed origin is explained by the analyticity at zero of our functions on one of the Riemann sheets.

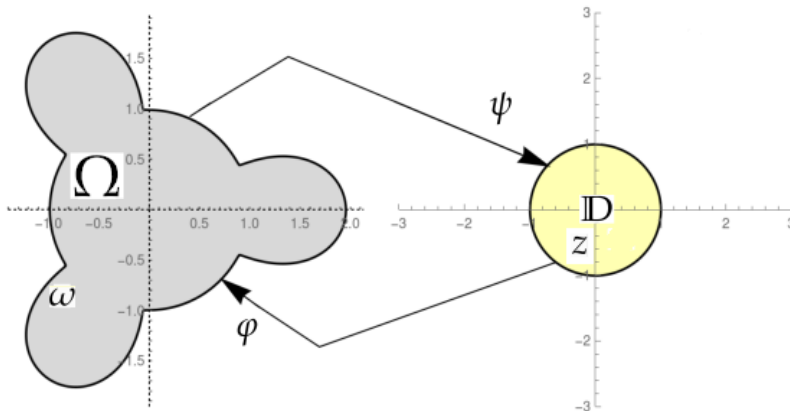


Figure 1: The map $z = \psi(\omega)$ from the simply connected Riemann surface Ω to the unit disk \mathbb{D} , and its inverse $\omega = \varphi(z)$.

to exactly one of the following: \mathbb{D}, \mathbb{C} or $\hat{\mathbb{C}}$ (see, e.g. [1, 2, 68]). Here, we mostly focus on Riemann surfaces uniformized on \mathbb{D} , as the latter two cases are too special [1], and also because their analysis would follow similar steps. See however Note 4.

We denote by ψ the conformal map of Ω onto \mathbb{D} , uniquely specified by $\psi(0) = 0, \psi'(0) > 0$, and write the inverse map $\psi^{-1} = \varphi$. See Figure 1. For the optimality Theorem 1, we define \mathcal{F}_Ω to be the family of functions F which are analytic on Ω . By M_F we denote the Maclaurin series of F , and $M_{F,n}$ will be the n th partial sum of M_F . An important role in our analysis is played by the natural metric on Ω , induced from the Poincaré disk, an elementary function of $|\psi|$. Our formulas are simpler in terms of $\rho = 1 - |\psi(\omega)|$, which we call the *conformal distance to the boundary of Ω* . This distance enters the convergence results in Theorem 1 for how the reconstruction depends on the number n of input terms in the input Maclaurin series $M_{F,n}$. We define φ^* by the right composition map: $\varphi^*F = F \circ \varphi$.

It will at times be convenient to consider shifts of sets in \mathbb{C} in which case we write $S + \zeta = \{\omega + \zeta : \omega \in S \subset \mathbb{C}\}$, and also to work with an inverted variable, changing the expansion point from $\omega = 0$ to $\omega = \infty$, in which case we write $1/S = \{1/\omega : \omega \in S \subset \mathbb{C}\} \subset \hat{\mathbb{C}}$.

In our discussion of resurgent functions, the singularities assume a simple form (cf. [19])

$$(\omega - \omega_0)^\alpha A(\omega) + B(\omega); \alpha \in \mathbb{C} \setminus \mathbb{Z}; \text{ or, for } \alpha \in \mathbb{Z}, \frac{d^k}{d\omega^k} [(\omega - \omega_0)^\alpha \ln(\omega - \omega_0) A(\omega)] + B(\omega) \quad (1)$$

for some $\alpha \in \mathbb{C}, k \in \mathbb{N}$, and where A, B are analytic at $\omega_0, A(\omega_0) \neq 0$. In this paper we refer to singularities of the type in (1) as *elementary singularities*. With this notation, important goals of our analysis are to learn as much as possible about the singularity locations ω_0 , the singularity exponent α , and the associated local functions A and B .

Theorem 1 constructs the best approximation of a function from its truncated Taylor series, within the family of functions having a common Riemann surface of analyticity Ω , and a common bound or rate of growth on Ω . This result only requires information about the Riemann surface Ω . Such *a priori* information exists for a wide class of functions encountered in analysis, the resurgent functions. In fact, for resurgent functions considerably more information, such as their singularity structure, is typically available. It is then possible to go well beyond the bounds provided in Theorem 1. Resurgent functions are analytic on the universal covering of \mathbb{C} with a discrete set of punctures, the locations and types of which are rigidly predetermined from the

equation (or even the type of equation) from which they originate [13, 19, 37]. Explicit examples and the application to the Painlevé equations is demonstrated in §3.

In cases where the uniformizing map is difficult to construct, the procedure in Theorem 1 can be adapted to extract information with near-optimal precision in restricted regions of Ω , for example near the singularities or boundaries, using simpler maps, see §4 and §5. These regions are usually the most important ones to study in mathematics and physics.

Even when such *a priori* analytic information is absent, we develop techniques to extract approximate information about the Riemann surface directly from the given truncated Taylor series, using standard analytical tools such as properly adapted techniques of conformal mapping, Borel summation and Padé approximants, and which can be refined to high precision using the new methods of *singularity elimination* (§4) and *approximate uniformization* (§5). We compare to the optimality result in order to quantify that these approximate methods are near-optimal.

In §6 we apply our methods and illustrate the main ideas on a number of examples important in applications. Appendix 7 contains details of some maps used in our analysis.

2 Optimality Theorem

The question of the best rate of convergence is not only natural, and interesting in itself, it is of substantial practical significance. Theorem 1 gives the optimal approximation of a function starting from its truncated Taylor series, within the family of all functions analytic on Ω , with common bounds on Ω . Specifically, the question answered by Theorem 1 is: what is the optimal approximation that can be obtained based on this general information at some point $\omega_0 \in \Omega$, as a function of ω_0 , and of the number n of input Maclaurin coefficients?

2.1 Discussion of the question and significance of Theorem 1

It may come as a surprise that evaluating the Taylor polynomial of a function $F \in \mathcal{F}_\Omega$ is *suboptimal*, even for points in $\mathbb{D} \subsetneq \Omega$ close to zero, so we start with some examples illustrating various important points.

Let us consider first the domain $\Omega_1 = \mathbb{C} \setminus [1, \infty)$ and let F be analytic in Ω_1 . From the n th root test it is clear that

$$|F(\omega) - M_{F,n}(\omega)|^{1/n} \sim |\omega|(1 + o(1)); \quad n \rightarrow \infty \quad (2)$$

This convergence rate can be improved in several ways. Suppose for simplicity that n is even. Then the diagonal Padé approximants $P_{F,n}$ of order $[n/2, n/2]$, uniquely defined by the first n Maclaurin series coefficients, converge faster (in the sense of logarithmic capacity: see §5):

$$|F(\omega) - P_{F,n}(\omega)|^{1/n} \sim \frac{1}{4}|\omega|(1 + o(1)); \quad n \rightarrow \infty; \quad |\omega| \text{ small} \quad (3)$$

In fact Padé approximants converge in capacity throughout Ω_1 at a geometric rate, as explained in §5. For functions analytic in Ω_1 having $[1, \infty)$ as a natural boundary, this gain of $\frac{1}{4}$ is optimal (this is the logarithmic capacity of the set $1/[1, \infty) = (0, 1]$, see §5). In this case, the leading order rate of convergence of Padé approximants in capacity is also optimal at any point of Ω_1 .

The same gain is obtained by the following conformal mapping procedure. Consider the biholomorphism $\varphi = z \mapsto 4z(1+z)^{-2}$, which maps \mathbb{D} onto Ω_1 , and let M_φ be its Maclaurin

series. Since φ^*F is analytic in \mathbb{D} , $M_{\varphi^*F,n}$ which equals $M_F \circ M_\varphi$ truncated to $o(z^n)$, also converges in \mathbb{D} and Theorem 1 below implies, after mapping back to Ω_1 (see Example 1 in §3),

$$|F(\omega) - M_{\varphi^*F,n} \circ \varphi^{-1}(\omega)|^{1/n} \sim \frac{1}{4}|\omega|(1 + o(1)); \quad n \rightarrow \infty; \quad |\omega| \text{ small} \quad (4)$$

Furthermore, the composition $M_{\varphi^*F,n} \circ \varphi^{-1}$ converges to F uniformly on compact sets in Ω_1 , at the same rate as the Padé approximants do in capacity, see §5.

When applied to domains in \mathbb{C} which are not necessarily maximal domains of analyticity, we refer to this conformal map procedure as the **Conformal-Taylor** method, CT. It has been used in applications [74, 14, 16]. We discuss CT and its precision in general, and in detail, in §5.3.

If instead we are dealing with functions analytic on covering of $\hat{\mathbb{C}} \setminus \{0, 1, \infty\}$ with fixed origin (cf. §1.1), then the constant $\frac{1}{4}$ in (4) becomes $\frac{1}{16}$. This follows from example 8 in §3, see (18) there.

For even simpler Riemann surfaces such as that of $F = \omega \mapsto \sqrt{1 - \omega}$, $\varphi(z) = 4z(1 + z)^{-2}$ is a uniformization map, $h(z) = \varphi^*F(z) = (1 + z)/(1 - z)$ is rational, and diagonal Padé approximants become *exact* in just one step: $P_n = h$ for all $n \geq 1$. This simple observation will be used later as an ingredient in our *singularity elimination* method which uses a combination of convolution operators and conformal maps (see §4).

2.2 The Optimal Rate Theorem on a Riemann Surface

Let Ω be as in §1.1 and $\omega_0 \in \Omega$. The following result constructs and characterizes $\hat{R}_n(\omega_0)$, the best approximant, in the sense stated in the Theorem, at ω_0 within the class of functions \mathcal{F} analytic on the same Riemann surface Ω . Let P be a polynomial of degree $n - 1$, our input truncated Maclaurin series.

Recall the maps shown in Figure 1. Theorem 1 shows that the best approximants are obtained by composing the input Maclaurin series with the series of φ truncated at the same order, summing the composed series, and then mapping back to Ω using ψ . Part 2 of Theorem 1 shows that optimality is sharper in the subclass of functions already well approximated by this procedure. Part 3 of Theorem 1 allows for functions that may grow as $\rho \rightarrow 0$ (i.e., as we approach the “boundary” of Ω).

Theorem 1. *Let Ω be a Riemann surface as in §1.1, $\omega_0 \in \Omega$, and P_n an $(n - 1)$ -order truncation of a Maclaurin series. We denote by \mathcal{F}_P the set of bounded functions on Ω to which P_n converges:*

$$\mathcal{F}_P = \{F \in \mathcal{F} : \|F\|_\infty < \infty, \text{ and } F(\omega) - P_n(\omega) = O(\omega^n) \text{ as } \omega \rightarrow 0\}$$

Let \hat{R}_n be the n -th Maclaurin polynomial, of degree $n - 1$, of the composed function φ^*P .

1. For $F \in \mathcal{F}_P$ we have

$$\frac{|F(\omega_0) - \hat{R}_n(\omega_0)|}{\|F\|_\infty} \leq \frac{(1 - \rho(\omega_0))^n}{\rho(\omega_0)} = \frac{|\psi(\omega_0)|^n}{1 - |\psi(\omega_0)|} \quad (5)$$

For every $R \in \mathbb{C}$ and $\delta > 0$ there exists $F_\delta \in \mathcal{F}_P$ so that

$$\frac{|F_\delta(\omega_0) - R|}{\|F\|_\infty} \geq (1 - \rho(\omega_0))^n(1 - \delta) \quad (6)$$

2. For $\varepsilon > 0$ let

$$\mathcal{F}_\varepsilon = \{F \in \mathcal{F}_P : F(\omega_0) \neq 0 \text{ and } |F(\omega_0)|^{-1}|F(\omega_0) - \hat{R}_n(\omega_0)| \leq \varepsilon\}$$

We have

$$\sup_{F \in \mathcal{F}_\varepsilon} \frac{|F(\omega_0) - \hat{R}_n(\omega_0)|}{|F(\omega_0)|} = \varepsilon \quad (7)$$

Assume n is large enough so that $\rho(\omega_0)^n < \varepsilon$. Then for every $R \in \mathbb{C}$ and every $\delta > 0$ there exists an $F_\delta \in \mathcal{F}_\varepsilon$ so that

$$\frac{|F_\delta(\omega_0) - R|}{|F_\delta(\omega_0)|} \geq \frac{1 - \delta}{1 + 2\varepsilon} \frac{|F_\delta(\omega_0) - \hat{R}_n(\omega_0)|}{|F_\delta(\omega_0)|} \quad (8)$$

3. Let $W = W_1 \circ (1 - \rho)$, where $W_1 : [0, 1) \rightarrow \mathbb{R}^+$ (a weight depending on the natural metric distance "to the boundary"). Define $\|\cdot\|_W$ by $\|F\|_W = \|F/W\|_\infty$, and let \mathcal{F}_W be the family of functions F analytic in Ω and such that $\|F\|_W < \infty$. Let $F \in \mathcal{F}_W \cap \mathcal{F}_P$. Then,

$$\frac{|F(\omega_0) - \hat{R}_n(\omega_0)|}{\|F\|_W} \leq (1 - \rho(\omega_0))^n \inf_{r \in (1 - \rho(\omega_0), 1)} \frac{W(r)}{r^{n-1}(r - (1 - \rho(\omega_0)))} \quad (9)$$

and for every $R \in \mathbb{C}$ and $\delta > 0$ there exists $F_\delta \in \mathcal{F}_W \cap \mathcal{F}_P$ so that

$$\frac{|F_\delta(\omega_0) - R|}{\|F_\delta\|_W} \geq (1 - \rho(\omega_0))^n \inf_{r \in (1 - \rho(\omega_0), 1)} \frac{W(r)}{r^n} (1 - \delta) \quad (10)$$

Proof. Note first that the map φ^* is an isometric isomorphism taking the space of analytic functions in Ω onto the space of analytic functions in \mathbb{D} , $L^\infty(\Omega)$ onto $L^\infty(\mathbb{D})$, and \mathcal{F}_W to \mathcal{F}'_W the space of functions in \mathbb{D} for which $\sup_{z \in \mathbb{D}} |F(z)/W(|z|)|$ is finite.

Moreover, since the composition of two C^n functions is C^n , the first n Maclaurin coefficients of F are in bijection to the first n Maclaurin coefficients of φ^*F . Hence the n th degree Maclaurin polynomial of φ^*F equals Q . Finally, $F(\omega_0) = (\varphi^*F)(\psi(\omega_0))$, and the optimality question is thus reduced to the case $\Omega = \mathbb{D}$. Hence, we can assume without loss of generality that $\Omega = \mathbb{D}$, and then φ is the identity, and $P = Q = \hat{R}$.

The proof in \mathbb{D} is elementary. The inequality (5) is simply obtained by taking the sup in the Cauchy formula

$$F(\omega_0) - \hat{R}(\omega_0) = \frac{\omega_0^n}{2\pi i} \oint \frac{s^{-n}F(s)}{s - \omega_0} ds \quad (11)$$

where the contour of integration is $\partial\mathbb{D}_r(0)$ with $r \in (|\omega_0|, 1)$ and letting $r \rightarrow 1$.

Let $R \in \mathbb{C}$. Consider functions in \mathcal{F}_P of the form $F_\lambda(\omega) = P(\omega) + \lambda\omega^n$ with $\lambda \in \mathbb{C}$. We have $\|F_\lambda\|_\infty^{-1}|F_\lambda(\omega_0) - R| = \|\lambda^{-1}P(\omega) + \omega^n\|_\infty^{-1}|\lambda^{-1}P(\omega_0) + \omega_0^n - \lambda^{-1}R|$ which, for $\lambda \rightarrow \infty$, converges to $|\omega_0|^n$, proving the optimality stated in (6).

To prove (7), it suffices to take $F(\omega) = \hat{R}_n(\omega) + c\omega^n$, with $c = \varepsilon\hat{R}(\omega_0)\omega_0^{-n}/(1 - \varepsilon)$.

For (8), consider the subfamily of \mathcal{F}_ε of functions of the form $F(\omega) = \hat{R}(\omega) + \alpha\tau\omega^n$, with $|\alpha| = 1$ and $\tau = \varepsilon\hat{R}(\omega_0)\omega_0^{-n}/(1 + \varepsilon)$ (included in \mathcal{F}_ε for small enough ε), for which we have

$$\frac{|F(\omega_0) - R|}{|F(\omega_0)|} = \frac{|\hat{R}(\omega_0) + \alpha\tau\omega_0^n - R|}{|\hat{R}(\omega_0) + \alpha\tau\omega_0^n|} \geq \frac{|\hat{R}(\omega_0) + \alpha\tau\omega_0^n - R|}{|\hat{R}(\omega_0)| + |\tau\omega_0^n|}$$

which, for α such that $\arg(\alpha\tau\omega_0^n) = \arg(\hat{R}(\omega_0) - R)$ is greater than

$$\frac{|\hat{R}(\omega_0) - R| + |\tau\omega_0^n|}{|\hat{R}(\omega_0)| + |\tau\omega_0^n|} \geq \frac{|\tau\omega_0^n|}{|\hat{R}(\omega_0)| + |\tau\omega_0^n|} = \frac{\varepsilon}{1 + 2\varepsilon}$$

Combined with (7), this implies (8).

For Part 3., recalling the isomorphism at the beginning of the proof, we use (11) and note that

$$\frac{1}{\|F\|_W} \frac{1}{2\pi} \left| \oint \frac{s^{-n} F(s) ds}{s - \omega_0} \right| \leq \inf_{r \in (|\omega_0|, 1)} \frac{W(r)}{r^{n-1}(r - |\omega_0|)}$$

where the contour of integration is $\partial\mathbb{D}_r(0)$ with $r \in (|\omega_0|, 1)$. This proves (9).

For (10) we proceed as in the proof of (6) and in the limit $\lambda \rightarrow \infty$ we obtain

$$\frac{|\omega_0|^n}{\|\omega^n\|_W} = \frac{|\omega_0|^n}{\sup_{r \in [0, 1]} r^n W(r)^{-1}} = |\omega_0|^n \inf_{r \in [0, 1]} \frac{W(r)}{r^n}$$

□

Note 2. Optimality in Theorem 1 is relative to the widest class of functions analytic on Ω and sharing a common rate of growth. Knowledge of more specific features of the functions, such as the concrete nature of their singularities, behavior towards infinity along special curves in Ω can lead to significant further improvements: see Sections 4, 5, 6. Such detailed information is available for resurgent functions, including the convergent ramified expansions near singularities at finite distance, asymptotic expansions at infinity and so on.

For instance, as will be shown in an applications paper [28], for the Borel transform of the tritronquée solution (see e.g. [17, 27]) of Painlevé P_I , using φ and $n = 200$ nonzero Maclaurin coefficients, we obtain the Stokes constant μ with about 12 digits of accuracy. With the same n , but using information about the singularity type at $\omega = \pm 1$ and singularity elimination, §4, we get 96 digits instead. See also note 11.

Note 3. 1. Let Ω be a domain in \mathbb{C} and $K = 1/(\Omega - \zeta)$, where $\zeta \notin \Omega$. If K is compact, then the constant $|\psi'(0)|$ is the logarithmic capacity (or trans-finite diameter) of K see [53, 65, 67] and §5. In this case $\text{cap}(K)$ measures the improvement of the rate of convergence for small ω_0 . For example, when $\Omega = \mathbb{C} \setminus [1, \infty)$, then $K = (0, 1]$, and $\text{cap}(K) = \frac{1}{4}$ is the factor in (3).

2. From the optimality in Theorem 1 it follows that $|\psi(\omega)| < |\omega|$ for $\omega \in \Omega$, and hence $\text{cap}(\Omega) < 1$. This means there is always an improvement over the convergence of the truncated series in (2).

The inequality above also follows in an elementary way. Since $\Omega \supset \mathbb{D}$ and $\psi(\Omega) = \mathbb{D}$, we have $|\psi| < 1$ in \mathbb{D} . Schwarz's lemma then implies $|\psi(\omega)| < |\omega|$ for all $\omega \in \mathbb{D}$ (or else ψ would be a rotation, contradicting our assumption that Ω is a strict superset of \mathbb{D}).

3. The approximations in Theorem 1 are expressed in terms of the conformal distance $\rho(\omega_0)$ of the point ω_0 to the boundary of Ω . When Ω is the universal cover of $\hat{\mathbb{C}}$ with a discrete set of punctures, then as ω_0 approaches a puncture, the uniformization map typically has a logarithmic singularity, since it has to locally accommodate the Riemann surface of a logarithm. Then, the Euclidean distance in \mathbb{C} to the puncture is exponentially larger than the conformal distance to the boundary. The result of this exponential distance distortion is a dramatic improvement in accuracy with respect to other methods of probing general singularities. See §6 for illustrative examples.

Note 4. In the case Ω is biholomorphically equivalent to \mathbb{C} and $F \in \mathcal{F}_\Omega$, the re-expanded series $M_F \circ M_\varphi$ converges in \mathbb{C} faster than geometrically. The rate of convergence of $M_F \circ M_\varphi$ at a point ω_0 is estimated from Cauchy's formula by $|\omega_0|^n \inf_{R>|\omega_0|} \sup_{|s|=R} |F(s)s^{-n-1}|$. A typical example is the uniformization of $\mathbb{C} \setminus \{1\}$ on \mathbb{C} , say for a function such as $F(\omega) = (1 - \omega)^a$, with $a \in \mathbb{C} \setminus \mathbb{Q}$. Here $\varphi(z) = (1 - e^{-z})$, and $\varphi^*F(z) = e^{-az}$, whose Maclaurin coefficients decrease factorially.

Note 5. 1. In many applications the underlying Riemann surface is the uniformization of $\hat{\mathbb{C}}$ with a discrete set of punctures, and moreover with special structure of the puncture positions. In such cases it is often possible to construct an explicit uniformization map. In this situation, there is a dramatic improvement over existing methods such as a Padé approximation, Conformal-Taylor and also over a Padé-Conformal approximation (Padé combined with a conformal map, not necessarily a uniformizing map). See for example the *tritonquée* solution of P_I in §6.2.

2. Some uniformization maps have elementary approximations (conformal maps of truncations of the Riemann surface, cf. §4-5), that are near-optimal and potentially simpler to use, see §3.2.

3 Uniformization of special Riemann surfaces, and conformal maps of special domains

We start with some known uniformization maps and their properties, and then construct new uniformization procedures needed in some applications of interest.

1. A simple but important case is the one-cut domain $\Omega = \mathbb{C} \setminus [1, \infty)$, for which

$$\psi(\omega) = \frac{1 - \sqrt{1 - \omega}}{1 + \sqrt{1 - \omega}} \quad \text{with inverse} \quad \varphi(z) = \frac{4z}{(1 + z)^2} \quad (12)$$

The optimal rate of convergence obtained from the Maclaurin series of a generic function F whose maximal analyticity domain is this Ω , and is continuous up to $\partial\mathbb{D}$ is, see (5),

$$|F(\omega_0) - \hat{R}_n(\omega_0)| \sim \frac{|\omega_0|^n}{2|\sqrt{1 - \omega_0}| |1 + \sqrt{1 - \omega_0}|^{2n-1}} \|F\|_\infty; \quad \omega_0 \in \Omega$$

The constant $C = 1/4$ in (3), the capacity of $1/\partial\Omega$, is simply $\psi'(0)$.

2. For the domain with two opposite cuts, $\Omega = \mathbb{C} \setminus (-\infty, -1] \cup [1, \infty)$, the maps are

$$\psi(\omega) = \sqrt{\frac{1 - \sqrt{1 - \omega^2}}{1 + \sqrt{1 - \omega^2}}} \quad \text{with inverse} \quad \varphi(z) = \frac{2z}{1 + z^2} \quad (13)$$

with $\psi(\omega) > 0$ for $\omega \in (0, 1)$. The capacity of $1/\partial\Omega$ is now $C = 1/2$. This construction generalizes straightforwardly to m symmetric cuts emanating from the vertices of a regular polygon. See Appendix 7 and [48]. This example also generalizes to $\Omega = \mathbb{C} \setminus (-\infty, -a] \cup [b, \infty)$: see (66) in Appendix 7.

Note 6. There is a more general principle behind (13) worth mentioning:

Lemma 7. Let Φ be a conformal map of \mathbb{D} to some domain $\mathcal{D} \subset \mathbb{C}$, and let $c = \Phi'(0) > 0$. Then, $\Phi_n(z) := \Phi(z^n)^{1/n}$ maps \mathbb{D} conformally to n symmetric copies of $\mathcal{D}^{1/n}$, i.e., to

$$\bigcup_{0 \leq j \leq n-1} e^{2\pi i j/n} \mathcal{D}^{1/n}$$

Proof. In a neighborhood of zero, Φ_n is uniquely defined by $\Phi_n(z) = |c^{1/n}|zH(z^n)$, where H is analytic at zero and $H(0) = 1$. Since $\Phi \neq 0$ on $\mathbb{D} \setminus \{0\}$, by the monodromy theorem, Φ_n extends analytically to \mathbb{D} . Since Φ is injective on \mathbb{D} , $\Phi_n(z) = \Phi_n(v)$ implies $z^n = v^n$. Now, $\Phi_n(z) = \Phi_n(v)$, written as $|c^{1/n}|zH(z^n) = |c^{1/n}|vH(v^n)$ implies $z = v$, and thus Φ_n is injective. Since Φ is onto \mathcal{D} , the rest follows from injectivity. \square

With proper adaptations, this construction extends to uniformization maps of Riemann surfaces.

3. For functions analytic on the universal covering Ω of $\hat{\mathbb{C}} \setminus \{-1, 1, \infty\}$ the maps are (compare with [38], p. 99)

$$\psi(\omega) = \frac{\mathbb{K}\left(\frac{1+\omega}{2}\right) - \mathbb{K}\left(\frac{1-\omega}{2}\right)}{\mathbb{K}\left(\frac{1-\omega}{2}\right) + \mathbb{K}\left(\frac{1+\omega}{2}\right)} \quad \text{with inverse} \quad \varphi(z) = -1 + 2\lambda\left(i\frac{1-z}{1+z}\right) \quad (14)$$

Here $\lambda = \theta_2^4/\theta_3^4$ is the elliptic modular function, θ_2, θ_3 are Jacobi theta functions, and $\mathbb{K}(m) = (\pi/2) {}_2F_1(\frac{1}{2}, \frac{1}{2}; 1; m)$ is the complete elliptic integral of the first kind of modulus $m = k^2$ [38]. The capacity is $C = \psi'(0) = \pi^{-2}\Gamma(\frac{3}{4})^4 \approx 0.2285$, more than a factor of two better than the capacity of the conformal map in eqn (13) of Example 2 above. Furthermore, $\hat{R}_n(\omega_0)$ in (5) converges on the whole universal covering of $\hat{\mathbb{C}} \setminus \{-1, 1, \infty\}$; that is, on all the Riemann sheets of the underlying function. See also Figure 2 and §6.4.

Note that the improvement in accuracy is particularly dramatic near singular points. Indeed, the leading order asymptotic behavior of ψ near $\omega = 1$ is $\psi(\omega) \sim 1 + 2\pi/\ln(1 - \omega)$. As a result of this log distortion, calculating a function after uniformization in the conformal disk at $z = 1 - 1/10$ results in evaluating it on Ω at $\omega \approx 1 - e^{-10 \times 2\pi} \approx 1 - 5 \times 10^{-28}$!

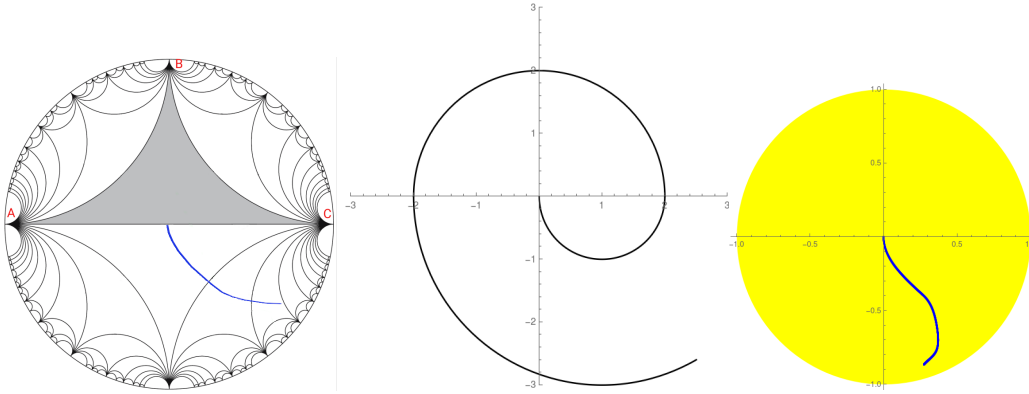


Figure 2: Uniformization of the universal cover Ω of $\hat{\mathbb{C}} \setminus \{-1, 1, \infty\}$ by the map φ in (14). The tessellation in the left-hand figure is adapted from [15]. Here the points A, B, C are mapped to $\{-1, \infty, 1\}$, respectively. The gray geodesic triangle in the Poincaré disk is conformally mapped by φ onto the upper half plane of Ω in the middle figure, and Schwarz reflections continue φ to the whole disk, with image onto Ω . The blue path in the disk is mapped to the spiral path in the middle figure on the universal cover Ω of $\mathbb{C} \setminus \{-1, 1\}$. The spiral is also the image of the blue curve in the right-hand figure, obtained as a composition of elementary maps, as discussed in §3.2.

4. The uniformization map for $\hat{\mathbb{C}} \setminus \{e^{-i\theta}, e^{i\theta}, \infty\}$, another important case in applications, is given by

$$\psi(\omega) = \frac{Z(\omega; \theta) - Z(0; \theta)}{1 - (Z(0; \theta))^* Z(\omega; \theta)}, \quad Z(\omega; \theta) \equiv \frac{\mathbb{K}\left(\frac{1}{2} + \frac{i}{2}\left(\frac{\omega}{\sin\theta} - \cot\theta\right)\right) - \mathbb{K}\left(\frac{1}{2} - \frac{i}{2}\left(\frac{\omega}{\sin\theta} - \cot\theta\right)\right)}{\mathbb{K}\left(\frac{1}{2} + \frac{i}{2}\left(\frac{\omega}{\sin\theta} - \cot\theta\right)\right) + \mathbb{K}\left(\frac{1}{2} - \frac{i}{2}\left(\frac{\omega}{\sin\theta} - \cot\theta\right)\right)} \quad (15)$$

The inverse is given in terms of the modular λ function by

$$\varphi(z) = e^{i\theta} - 2i \lambda \left(i \left(\frac{\mathbb{K}\left(\frac{1}{2} - \frac{i}{2}\cot\theta\right) - \mathbb{K}\left(\frac{1}{2} + \frac{i}{2}\cot\theta\right)z}{\mathbb{K}\left(\frac{1}{2} + \frac{i}{2}\cot\theta\right) + \mathbb{K}\left(\frac{1}{2} - \frac{i}{2}\cot\theta\right)z} \right) \right) \quad (16)$$

These maps are obtained from (14) by a suitable Möbius transformation and disk automorphism.

5. It is straightforward to generalize the two previous examples to the universal covering of $\hat{\mathbb{C}} \setminus \{\omega_1, \omega_2, \infty\}$, where $\omega_1, \omega_2 \in \mathbb{C}$. The uniformization maps are again expressed in terms of the elliptic function \mathbb{K} and the elliptic modular function λ . The important case in the previous example, with two complex conjugate points, $\omega_1 = e^{i\theta} = 1/\omega_2$, which occurs in many applications, is discussed further in §6.3.2.

6. For uniformization of other Riemann surfaces based on the universal covering of $\hat{\mathbb{C}} \setminus \{-1, 1, \infty\}$ possessing a nontrivial fundamental group see for example [38], §2.7.2. See also [48] for a collection of explicit uniformization maps of $\hat{\mathbb{C}} \setminus S$ where S is a finite set of points in $\hat{\mathbb{C}}$, including for example $S = \{-1, 0, 1, \infty\}$, $S = \{-3, -1, 0, 1, 3, \infty\}$ and $S = \{0, 1, e^{\pi i/3}, \infty\}$, and when S consists of the n -th roots of unity. Algebraic functions have compact Riemann surfaces, and some explicit uniformizing maps can be found in Schwarz's table in [38].

7. In certain special cases the uniformizing map produces a meromorphic or rational function, in which case a subsequent Padé approximation becomes exact. For example, the function $F(\omega) = \sqrt{1-\omega}$ has a compact Riemann surface Ω (as all algebraic functions do). The uniformizing map $\omega = \varphi(z) = 4z/(1+z)^2$ makes φ^*F meromorphic, $\varphi^*F(z) = (1-z)/(1+z)$, hence analytic on the Riemann sphere, and Padé $[n, n]$ is exact for $n > 0$. A more sophisticated example is the Riemann surface Ω of functions with three square root branch points, which is uniformized by $(z^2 - 1)^2/(z^2 + 1)^2$, [38], and the functions become rational; the uniformization theorem brings Ω to $\hat{\mathbb{C}}$. This is another case where Padé becomes exact.

8. The following uniformization is described in [59], p. 323. However, we provide here a more precise mathematical description of the Riemann surface, and a shorter proof. Let Ω be the Riemann surface with fixed origin of $\hat{\mathbb{C}} \setminus S$, with $S = \{0, 1, \infty\}$. Then the conformal map $\psi : \Omega \rightarrow \mathbb{D}$ is the *elliptic nome* function q :

$$\psi(\omega) = q(\omega) = e^{-\pi \frac{\mathbb{K}(1-\omega)}{\mathbb{K}(\omega)}} \quad (17)$$

and φ is the *inverse elliptic nome* function. We have for small z

$$\varphi(z) = 16z - 128z^2 + 704z^3 + \dots \quad (18)$$

Proof. We start with the well known uniformization over the upper half plane \mathbb{H} of the universal cover of $\hat{\mathbb{C}} \setminus \{0, 1, \infty\}$ by $\tau(\omega) = i\mathbb{K}(1-\omega)/\mathbb{K}(\omega)$, see [38], p 99. Note that $q = e^{\pi i \tau}$. The map τ is also conformal between \mathbb{H} and the geodesic triangle Δ , see Fig. 3. The inverse function, $\lambda = \tau^{-1}$ is the modular elliptic function. The set $T = e^{\pi i \Delta}$ is the curvilinear triangle T in Figure 3, where the upper side is an analytic curve. We aim to show that $W = q^{-1}$ extends analytically to \mathbb{D} by successive Schwarz reflections of T , and its reflections, across their sides. We also note that with $\omega \in T$ we have $W(z) = \lambda(\frac{1}{\pi i} \log z)$. Since λ is analytic in the upper half plane, W admits analytic

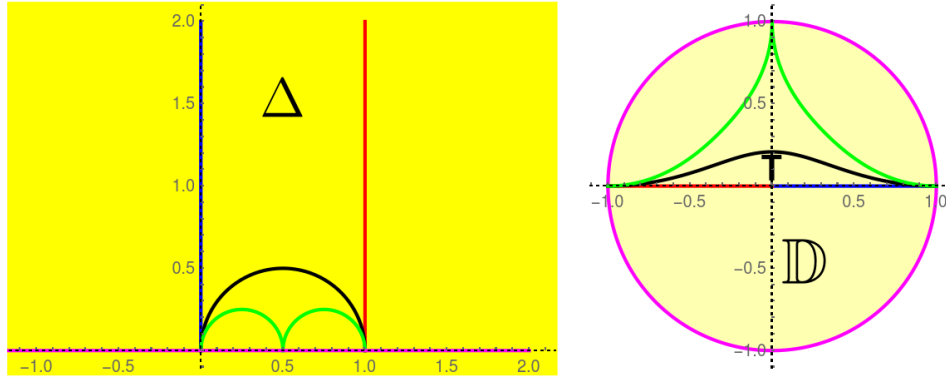


Figure 3: Images of geodesic triangles in \mathbb{H} through $h(\omega) = \omega \mapsto e^{\pi i \omega}$. Like-colored pieces of the boundaries correspond to each other through h .

continuation through the rays above. Using the periodicity property $\lambda(t+2) = \lambda(t)$ we see that the monodromy of W around zero is trivial. Furthermore, the product representation of λ for $\Im \omega > 0$,

$$\lambda(\omega) = 16e^{\pi i \omega} \prod_{k=1}^{\infty} \left(\frac{1 + e^{2k\pi i \omega}}{1 + e^{(2k-1)\pi i \omega}} \right)^8$$

shows that $\lim_{t \rightarrow i\infty} \lambda(t) = 0$, hence $z = 0$ is a point of analyticity of W , and $W(0) = 0$. Each Schwarz reflection of T mirrors Schwarz reflections of Δ . It is clear that the set of all these reflections cover \mathbb{D} since $e^{\pi i \mathbb{H}} = \mathbb{D}$ and, as in the uniformization proof for λ , the reflections of Δ cover \mathbb{H} . The curves starting at zero on the universal cover of $\hat{\mathbb{C}} \setminus \{0, 1, \infty\}$ correspond to curves in \mathbb{D} . \square

- Note 8.**
1. This Ω in example 8 is distinct from the universal covering of $\hat{\mathbb{C}} \setminus \{-1, 1, \infty\}$ considered in example 3 above, since Ω in example 8 is a covering with fixed origin; the functions living on Ω are analytic at zero on one sheet and may be singular there on all others.
 2. The reflection of 0 across the curvilinear side of T is i , and successive reflections carry it to the binary rational angles. Thus, zero becomes inaccessible on “higher Riemann sheets”.

As an example, Fig. 4 shows the singularities on the Riemann surface of the complete elliptic integral $\mathbb{K}(\omega)$, seen after uniformization through φ in (18), with 200 nonzero terms of the right-composition $\varphi^* \mathbb{K}$. We note that the only possible singularities of \mathbb{K} on any Riemann sheet are $\{0, 1, \infty\}$. The large number of singularities visible in Fig. 4 is a reflection of the large number of “deep” Riemann sheets visible after uniformization; more details are given in the caption.

3.1 Uniformization in the Borel plane of Painlevé Equations

Let $\Omega_{\mathbb{Z}}$ be the set of equivalence classes of curves starting at 0, modulo homotopies in $\mathbb{C} \setminus \mathbb{Z}$.⁴ Then $\Omega_{\mathbb{Z}}$ is the universal cover for the Borel transforms of the (divergent, normalized) asymptotic series of the tritronquée solutions of the Painlevé $P_I - P_V$ equations [19]. Figure 5 shows the singularity structure of Y , the Borel transform of the tritronquée solution y of Painlevé P_I , on its Riemann surface. Starting from a finite number of terms of the asymptotic expansion,

⁴Not $\hat{\mathbb{C}} \setminus \mathbb{Z} \setminus \{\infty\}$; a curve around infinity is undefined, since \mathbb{Z} is not compact.

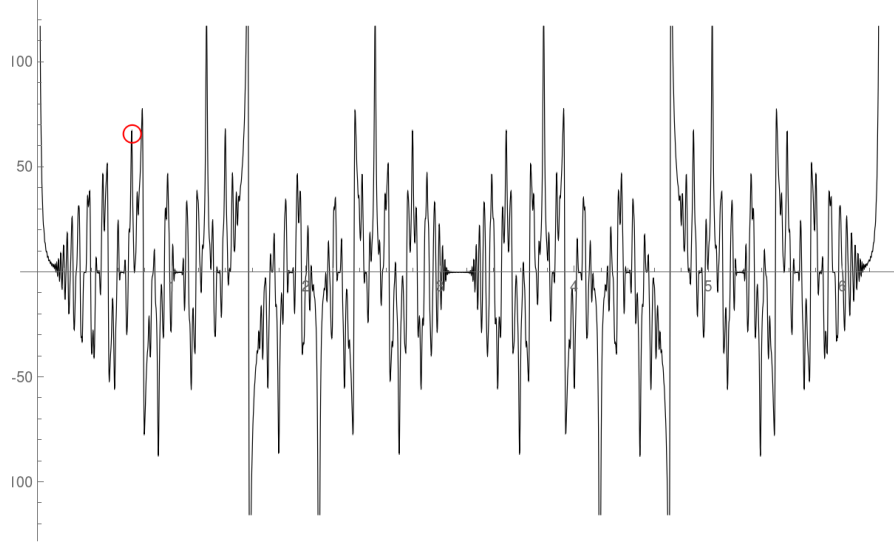


Figure 4: A plot of $\varphi^*\mathbb{K}$ on a circle of radius 0.997 using as input 200 nonzero terms of its Maclaurin series. The marked singularity is at 0, after a clockwise loop around 1 and a clockwise loop around ∞ . The higher the Riemann sheet, the more suppressed is the singularity. Properly dilated, the singularities exhibit a periodic structure, reflecting the simple monodromy group of \mathbb{K} . Compare with Fig. 5, the Riemann surface of the Borel transform of the tritronquée of P_I which has infinitely many singularities on each Riemann sheet, and exhibits a less regular structure.

the uniformization of the associated Riemann surface described in Theorem 9 permits analytic continuation onto the higher sheets of this Riemann surface.

Theorem 9. $\Omega_{\mathbb{Z}}$ is uniformized by $\psi = \varphi^{-1}$, where $\varphi = \frac{1}{2\pi i} \ln(1 - q^{-1})$, with q the elliptic nome function, as in (17).

See Fig. 5, and also Fig. 2.

Proof. This result follows from example 8 of the previous section (see equations (17) and (18)), and the following lemma.

Lemma 10. The function $\Phi = \omega \mapsto \frac{1}{2\pi i} \log(1 - \omega)$ maps conformally the surface Ω in example 8 of the previous section onto $\Omega_{\mathbb{Z}}$.

Proof. Let \mathcal{G} be the free group with generators r_k , where for $k \in \mathbb{Z}$ r_k is the anticlockwise rotation around k . An equivalence class of curves of $\Omega_{\mathbb{Z}}$ can be described by a word $r_{k_1} \cdots r_{k_m}$, for some m plus a piecewise linear arc in \mathbb{C} . Let \tilde{r}_0, \tilde{r}_1 the generators of the group of Ω . The result follows by noting that the element $r_k \in \mathcal{G}$ is obtained through Φ from $\tilde{r}_0 \tilde{r}_1^k$. Injectivity is clear. (In words, through Φ , any “address” in $\Omega_{\mathbb{Z}}$ can be reached uniquely from an address on Ω .) \square

\square

Note 11. 1. Denoting by Y the Borel transform of the tritronquée solution y of Painlevé P_I , an n -th root test on φ^*Y shows that its Maclaurin coefficients grow roughly like $e^{2\sqrt{n}}$ which implies exponential growth towards the boundary of the conformal disk. Importantly, Y does not have exponential growth on any particular Riemann sheet but there is substantial

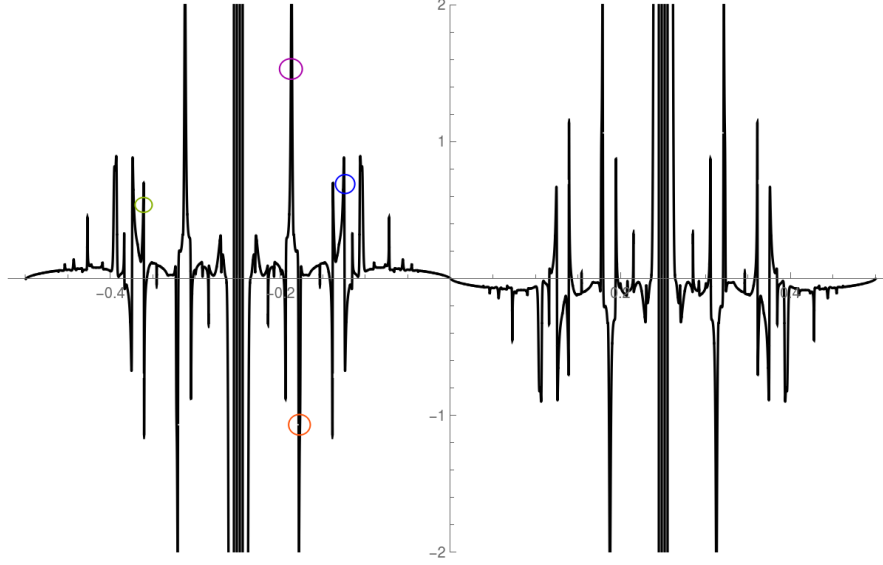


Figure 5: Singularities of φ^*Y along the conformal circle, where Y is the Borel transform of the tritronquée solution y of Painlevé P_1 , whose Riemann surface is covered by φ in Theorem 9. We used $n = 200$ nonzero terms of the asymptotic expansion of y , after Borel transform. The singularities depicted correspond to those of Y at -2 , reached by analytic continuation from below (green) -1 after analytic continuation around $+1$ (magenta), 0 after analytic continuation around $+1$ (red) and -2 reached from above. The thick lines represent a cumulative effect of all sheets in some directions, see the discussion in Note 11, part 1.

strengthening of the singularities at $\pm n$ on the n -th sheet, [19], which results in cumulative exponential growth on Ω , giving the two thick lines on the graph.

In this sense φ^*Y can see the totality of the Riemann surface, even with 200 terms of the series.

2. The map in Theorem 9, optimal for otherwise featureless functions, is suboptimal for essentially any particular singularity of Y , including infinity on a given Riemann sheet. As for a general resurgent function, detailed information is available about each singularity. Singularity elimination (see §4) applies to Y , and is far more accurate for singularities at finite distance, and specific methods perform much better at infinity as well.
3. Resurgent functions have an infinite set of resurgence relations, so the actual Riemann surface of Y is $\Omega_{\mathcal{G}} = \mathbb{R}_{\mathbb{Z}}/\mathcal{G}$ where \mathcal{G} would be the group of relations, and in all likelihood uniformizing $\Omega_{\mathcal{G}}$ explicitly is beyond reach. However, these relations are contained in the shape of singularities, so singularity elimination (as discussed in §4) should achieve an optimal, or near-optimal final result.

3.2 Uniformization by composition of conformal maps for domains in \mathbb{C} .

We demonstrate this procedure with an example. Let ψ_1 and φ_1 be the maps in (12), and define $\psi_n(\omega) = [\psi_1(\omega^n)]^{1/n}$, with inverse $\varphi_n(z) = [\varphi_1(z^n)]^{1/n}$, for $n \in \mathbb{Z}$, with the usual branch choices.

Theorem 12. *The composition map $\psi_{2^n} \circ \psi_{2^{n-1}} \circ \dots \circ \psi_1(\omega)$ converges, as $n \rightarrow \infty$, to $\psi(\omega)$ in (17), the elliptic nome function.*

Proof. We first note that the singular points of ψ_k are $\{0, \{\sigma_j\}_{j \leq k-1}, \infty\}$, where $\{\sigma_j\}_{j \leq k-1}$ are the k -th roots of unity (with zero a point of analyticity on the first Riemann sheet). Secondly, for any $n \in \mathbb{N}$, $\psi_{2^n} \circ \psi_{2^{n-1}} \circ \dots \circ \psi_1$ is only singular at $\{0, 1, \infty\}$ (with zero a point of analyticity on the first Riemann sheet); this follows immediately by examining the singularities of φ_k for $k \in \mathbb{N}$. Convergence of the composition follows from the fact that $\psi_k = 2^{-2/k} \omega(1 + O(\omega^k))$ (see also the proof of Lemma 13).

Next, we note that the non-constant term of the Puiseux expansion of ψ_n at the finite nonzero singularities is of the form $\sigma_j + \text{const} \sqrt{\omega - \bar{\sigma}_j}(1 + o(1))$, and $1 + \text{const} \cdot \omega^{-1/2}(1 + o(1))$ at infinity. We describe the monodromy group of ψ_k in terms of the generators r_{σ_j} and r_∞ . A straightforward calculation shows that any of the elements $r_{\sigma_j}^2, r_\infty^2, r_\infty r_{\sigma_j}$ of the monodromy group of the Riemann surface of ψ_k is mapped on a single r_{σ_j} or r_∞ of the monodromy group of the Riemann surface of ψ_{2^k} , while $r_\infty r_{\sigma_j}$ for $i \neq j$ is mapped inside \mathbb{D} . Injectivity of the limit map is also straightforward.

An alternative proof, based on convergence to q^{-1} is given in Lemma 13 below. \square

Lemma 13. 1. We have

$$\varphi_1 \circ \varphi_2 \circ \varphi_4 \circ \dots \circ \varphi_{2^k} \rightarrow q^{-1} \quad , \quad k \rightarrow \infty \quad (19)$$

uniformly in \mathbb{D} .

2. Moreover, starting the doubling iteration with φ_n instead of φ_1 , we have more generally

$$\varphi_n \circ \varphi_{2n} \circ \varphi_{4n} \circ \dots \circ \varphi_{2^k n} \rightarrow z \mapsto [q^{-1}(z^n)]^{1/n} \quad , \quad k \rightarrow \infty \quad (20)$$

which uniformizes the covering with fixed origin of $\hat{\mathbb{C}} \setminus S$ where S are the n -th roots of unity.

Proof. We note that $z(\omega)$ is analytic in the unit disk (see also (18)).

The Landen transformation [38] implies that the map $\varphi_1(\omega)$ satisfies $\varphi_1(w(z^2)^{1/2}) = w(z)$, and therefore $w(z^2)^{1/2} = \varphi_1^{-1}(w(z))$. Iterating this identity, we find in general, for $m \in \mathbb{N}$ and $z \in \mathbb{D}$, that

$$w(z^{2^{m+1}})^{1/2^{m+1}} = \varphi_{2^m}^{-1} \circ \dots \circ \varphi_1^{-1}(w(z))$$

For any function analytic within the unit disk and such that $f(z) = cz(1 + o(z))$, and for any $r < 1$ we have $\lim_{n \rightarrow \infty} f(z^n)^{1/n} = z$ uniformly in $\mathbb{D}_r(0)$ (since $f(z)/z$ is uniformly bounded there). This implies

$$\lim_{m \rightarrow \infty} \varphi_{2^m}^{-1} \circ \dots \circ \varphi_1^{-1}(w(z)) = z$$

The result (19) follows by straightforward function inversions. The proof of (20) for general n is very similar. The proof of (21) follows by noting that $\varphi_n(\omega) = \varphi_1(\omega^n)^{1/n}$. \square

Note 14. 1. The limit in Lemma 13 can also be expressed as an infinite iteration limit of the ascending Landen transformation, $L(z) = 2\sqrt{z}/(1+z)$:

$$\lim_{k \rightarrow \infty} L \circ L \circ \dots \circ L(z^{2^k}) = \sqrt{q^{-1}(z^2)} \quad (21)$$

2. This result has an important practical implication: we can approximate a complicated (e.g., elliptic) map by a composition of elementary (e.g., rational) maps. For example, the right-hand figure of Fig. 2, shows the result of a **finite** number of iterations of the elementary maps φ_n . The spiral path on the universal cover Ω of $\mathbb{C} \setminus \{-1, 1\}$ in the middle figure is the image of the blue curve in the right-hand figure under the six-step composition of elementary maps $\varphi_2 \circ \varphi_4 \circ \varphi_8 \circ \dots \circ \varphi_{64}$. Thus, these elementary rational maps enable one to explore a finite number of Riemann sheets. See also §6.4.

4 Singularity elimination.

The principal motivation underlying the analysis in this section is to develop new methods to give precise determinations of the location and nature of a chosen singularity, and information about the behavior of the function near the singularity. The main application of this procedure is to explore the singularities of resurgent functions, which have *elementary singularities* of the form in (1).

For such functions, we show that there exist operators that regularize the singularities, in the sense of transforming them into points of analyticity. This allows for a detailed and precise analysis of the singularity structure, type, and local expansions. In general, these operations cannot be reduced to conformal maps. For example, a function with a singularity of the type $\log(1 - \omega)A(\omega) + B(\omega)$, with A, B holomorphic at $\omega = 1$, cannot be composed with a holomorphic map φ with $\varphi(0) = 0, \varphi(1) = 1$ such that the composition is analytic at $\omega = 1$. The proof is straightforward⁵. Uniformizing the surface of the log at $\omega = 1$ results in moving the singularity from 1 to infinity. However, it is possible to construct linear operators which simply remove the log singularity, without “moving” the points 0, 1. That these methods are distinct from uniformization also follows from the fact that any function of the form

$$\sum_{k=1}^N c_k (\omega - \omega_k)^\alpha \quad (22)$$

(with a common exponent α) can be reduced to a rational one by the simple procedures described below, but its Riemann surface is not uniformizable by any simple map for general ω_k .

4.1 Properties of convolution and the singularity elimination procedure

In this section we analyze the general structure of singularities of Laplace convolution, see (23), and describe the process of elimination of elementary singularities of type (1). We begin with some definitions and the description of the procedure. We also analyze the singularities of convolutions of general analytic functions F, G in the neighborhood of the singularities of F, G .

Definition 15. Laplace convolution of F and G is defined as

$$(F * G)(\omega) = \int_0^\omega F(s)G(\omega - s)ds \quad (23)$$

Note 16. 1. For $\Re\beta > -1$, an important role is played by the linear operator L_β of convolution with ω^β , followed by multiplication by $\omega^{-\beta}$:

$$(L_\beta F)(\omega) = \omega^{-\beta} \int_0^\omega F(s)(\omega - s)^\beta ds \quad (24)$$

As shown below in Lemma 17 and Lemma 23, if F is analytic in \mathbb{D} with an elementary singularity of type (1) at ω_0 , then $L_\beta F$ is also analytic in \mathbb{D} with an elementary singularity of type (1), where α is replaced by $\alpha + \beta + 1$. In other words, the convolution operator L_β in (24) allows us to modify the nature of the chosen singularity.

⁵Indeed, taking $A = 1, B = 0$, and then $A = 1$ and $B(\omega) = \omega$, we see that φ must be analytic at 1, hence $\varphi(1 + s) = 1 + o(s)$. But then $\log(1 - \varphi)$ is unbounded at 1.

2. Let us normalize so that the chosen singularity is at $\omega_0 = 1$. For singularity elimination, it is convenient to choose β so that $\alpha + \beta + 1 = k/2$, for some nonnegative odd integer k , so that the singularity of $L_\beta F$ becomes a square-root branch point

$$(L_\beta F)(\omega) = (1 - \omega)^{1/2} A_1(\omega) + B_1(\omega) \quad (25)$$

in a neighborhood of 1 where A_1, B_1 are analytic at 1.

3. Let φ denote a conformal map of the unit disk \mathbb{D} to some Riemann surface Ω , mapping 0 to 0, and 1 to 1, and such that $(\varphi - 1)$ has a double zero at $z = 1$. Simple examples of such maps are

$$\varphi_0(z) = 2z - z^2; \quad \varphi_1(z) = \frac{4z}{(1+z)^2}; \quad \text{and} \quad \varphi_2(z) = \frac{2z}{1+z^2} \quad . \quad (26)$$

Ideally, such a map would take part of the domain of analyticity of F to the unit disk, ensuring convergence of $\varphi^*(L_\beta F)(\omega)$.

4. Replacing in (25) ω by any $\varphi(\omega)$ for any φ in (26) we see that $\varphi^*(L_\beta F)(\omega)$ is now analytic at both $\omega = 0$ and $\omega = 1$.

5. The inverse functions of the maps above are elementary, and inverting $\varphi^*(L_\beta F)$ results in a special function series representation of F . But even if, for a more complicated φ , inverting convolution can only be done by some (convergent in the limit) numerical scheme, we reiterate that the purpose here is to most accurately recover an unknown F from truncated Maclaurin series, and not to provide economical approximations of a known function.

6. Lemma 20 applies to much more general singularities than the elementary singularities in (1), and can be used for their elimination. However, in this paper we will not attempt to classify in general the singularities that can be eliminated.

4.2 Singularity Transformation

Lemma 17 (Preservation of Riemann surfaces by L_β). *Assume Ω is a covering with fixed origin of $\mathbb{C} \setminus S$, and $0 \notin S$ ⁶. We generalize L_β when $\Re\beta > -1$, by interpreting the convolution in (24) as an integral along a smooth curve $\gamma : [0, 1] \rightarrow \Omega$ with $\gamma(0) = 0$ and $\gamma(1) = \omega$.*

Then, if F is analytic on Ω , $L_\beta F$ is also analytic on Ω .

Proof. Analyticity in \mathbb{D} is easily shown by replacing F by M_F , and then using dominated convergence to integrate term by term M_F . Then we calculate

$$L_\beta \left(\sum_{k=0}^{\infty} a_k \omega^k \right) = \sum_{k=0}^{\infty} \frac{\Gamma(\beta+1)\Gamma(k+1)}{\Gamma(\beta+k+2)} a_k \omega^{k+1} \quad ; \quad |\omega| < 1 \quad (27)$$

For large k we have

$$\frac{\Gamma(k+1)}{\Gamma(\beta+k+2)} = O(k^{-1-\beta})$$

implying that analyticity in \mathbb{D} is preserved.

Next, examining (24) we interpret $F(s)ds$ as a bounded complex measure along any path from 0 to ω and note that the integrand, and hence the integral over γ are manifestly analytic at all points in $\gamma([0, 1])$. Let $\varepsilon > 0$ be such that $\mathbb{D}_{2\varepsilon}(\omega) \subset \Omega$, let $\omega_1 \in \mathbb{D}_\varepsilon(\omega) \in \gamma([0, 1])$ and write the integral along γ as $\int_0^\omega = \int_0^{\omega_1} + \int_{\omega_1}^\omega$. The first integral is analytic by the argument above.

⁶In other words, the curves in Ω start from zero and do not cross zero again unless they are homotopic to a point.

The second integral can be replaced by a straight line integral from ω_1 to ω , where we change variable $s = \omega - t$ to get

$$\int_0^{\omega - \omega_1} F(\omega - t)t^\beta dt$$

which is analytic since F is analytic in $\mathbb{D}_{2\varepsilon}(\omega)$ □

Note 18. Convolving more general functions with singularities **alters** the Riemann surface, in general. For instance $(1 - \omega)^{1/2} * (1 - \omega)^{1/2}$, is an elementary function with a square root type singularity at 1 and a log-type singularity at 2. We refer to [61] for the theory of the location of singularities generated via convolution.

For analyzing the **type** of singularities of $F * G$ for more general F, G we restrict our attention to star-shaped domains $\mathcal{N} \supset \mathbb{D}$ (meaning that for each point in \mathcal{N} , the line segment connecting it to 0 is also in \mathcal{N})

Lemma 19 (Analyticity of Convolution). *Let $\mathcal{N} \supset \mathbb{D}$ be a star-shaped domain in \mathbb{C} . If F and G are analytic in \mathcal{N} , then so is $F * G$.*

Proof. This is clear if we interpret $F(s)ds$ in (23) as a finite complex measure on compact sets of \mathcal{N} . □

The next Lemma describes how singularities at 0 and ω_0 interact. For simplicity of notation, we **normalize** ω so that $\omega_0 = 1$.

Lemma 20 (Calculation of singularities of convolution). *1. Assume F is analytic in a neighborhood of $(0, 1 + \varepsilon]$, possibly singular at zero but $F \in L^1((0, 1 + \varepsilon))$, G is analytic in a neighborhood of $[0, 1 + \varepsilon] \setminus [1, 1 + \varepsilon]$ with continuous lateral limits (possibly different) on the cut. Assume further that there exist two functions, S analytic in $\mathbb{D}_\varepsilon(1) \setminus [1, 1 + \varepsilon]$, and B_1 is analytic in the disk $\mathbb{D}_\varepsilon(1)$ such that*

$$(F * G)_1(\omega) := \int_1^\omega F(\omega - s)G(s)ds = S(\omega) + B_1(\omega) \quad (28)$$

Then,

$$\int_0^\omega F(\omega - s)G(s)ds = S(\omega) + B(\omega) \quad (29)$$

where $B(\omega)$ is analytic in $\mathbb{D}_\varepsilon(1)$.

The result can be adapted to the case where instead $G = G_1^{(k)}$ for some $k \in \mathbb{N}$, and G_1 satisfies the assumptions of the lemma.

2. The result extends to Riemann surfaces Ω as in Lemma 17 if $F(\omega) = \omega^\beta$, $\Re\beta > -1$. More precisely, recalling that we normalized ω_0 so that its projection on \mathbb{C} is 1, we choose a line segment in Ω emanating from ω_0 whose projection in \mathbb{C} is $[1, 1 + \varepsilon)$ and replace the branch jump across $[1, 1 + \varepsilon)$ by the branch jump across this segment.

Proof of Lemma 20. 1. We note that the jumps across the cut $[1, 1 + \varepsilon)$ of $\int_0^\omega F(\omega - s)G(s)ds$ and of S must coincide, and it evidently also coincides with the jump across the cut⁷ $[1, 1 + \varepsilon)$ of $\int_1^\omega F(\omega - s)G(s)ds$ (since the integrand is analytic in \mathbb{D} . Using Lemma 19 and the assumptions of Lemma 20, we see that $B(\omega) := \int_0^\omega F(\omega - s)G(s)ds - S(\omega)$ is analytic in $\mathbb{D}_\varepsilon(1) \setminus [1, 1 + \varepsilon]$ and continuous in $\mathbb{D}_\varepsilon(1)$, and Morera's theorem implies that B is analytic in $\mathbb{D}_\varepsilon(1)$.

⁷As usual, by "jump across the cut" we mean the upper limit minus the lower limit along the cut.

For a general k we write $\int_0^\omega = \int_0^{1/2} + \int_{1/2}^\omega$. In the second integral we integrate by parts k times to eliminate the derivatives of G_1 and apply the first part.

2. Follows in the same way, noting that only a neighborhood of ω_0 is involved in both the statement and in the proof of 1. \square

Note 21. Lemma 20 is a “localization” lemma, whose point is that $S(\omega)$ can be calculated from local expansions of F and G at 0 and 1 respectively, whenever such expansions exist⁸, since $\int_1^\omega F(\omega - s)G(s)ds$ only depends on these local expansions.

Note 22. 1. Clearly, for the elementary singularities of type (1), the local expansion assumed in (28) always exists. (Note that other singularities of F and G , including subtler singularities on the second Riemann sheet, may mean that the local expansion of F at zero and that of G at 1 have radius of convergence < 1 .)

2. The convolution operator L_β is important in applications, as it gives a simple way to transform the nature of the singularity. Lemma 23 below shows that the effect of this operator can be implemented directly on the original expansion coefficients.

3. The transformation of singularities can also be understood in terms of fractional derivatives, as is clear from the representation in (24). See [5] for an application to Borel transforms.

Lemma 23. *Assume F is analytic in \mathbb{D} , and at $\omega = 1$ it has an elementary singularity of type (1). Then, for $\Re\beta > -1$ the convolution $L_\beta F$ in (24) has an elementary singularity of type (1) with α replaced by $\alpha + \beta + 1$.*

Proof. We rely on Lemma 20. Take first $\alpha \notin \mathbb{Z}$. In view of the second part, we may assume $\Re\alpha > -1$. In our case, for small enough t ,

$$S(\omega) = -2i \sin(\pi\alpha)(1 - \omega)^{\beta+\alpha+1} \int_0^1 (1 - t)^\beta t^\alpha A(1 + t(1 - \omega)) + B_1(\omega) \quad (30)$$

as seen by the change of variable $s = t\omega$. Writing near 1, the local expansion $A(\omega) = \sum_{k=0}^\infty a_k(1 - \omega)^k$ and inserting in (30), we see that

$$S(\omega) = (1 - \omega)^{\beta+\alpha+1} \sum_{k=0}^\infty a_k \frac{\sin(\alpha\pi)\Gamma(\beta + 1)\Gamma(\alpha + k + 1)}{\Gamma(\beta + \alpha + k + 2) \sin((\beta + \alpha)\pi)} (1 - \omega)^k \quad (31)$$

proving the assertion in this case. (Note the obvious analogy to singularities of hypergeometric functions.)

For a logarithmic singularity, $F(\omega) = \ln(1 - \omega)A(\omega) + B(\omega)$, we have

$$(L_\beta F)(\omega) = \omega^{-\beta} \int_0^\zeta (\zeta - u)^\beta \ln(-u) A(1 + u) du \quad , \quad \zeta = \omega - 1 \quad (32)$$

and the jump across the cut of $L_\beta F$ is

$$S(\omega) = 2\pi i \omega^{-\beta} \int_0^\zeta (\zeta - u)^\beta A(1 + u) du \quad (33)$$

⁸Very generally, even in the absence of local expansions, Plemelj’s formulas [2] give a local representation $S(\omega)$ in the form $\frac{1}{2\pi i} \int_0^{1+\epsilon} (\omega - \tau)^{-1} \int_1^\lambda F(\lambda - s)\Delta G(s)dsd\tau$, where ΔG is the jump across the cut of G .

Writing $A(\omega) = \sum_{k=0}^{\infty} a_k(1-\omega)^k$ near 1, one can verify that, in order to achieve the same branch jump with an S having a cut $[1, \varepsilon)$ we define $S(\omega) = 2\pi i \omega^{-\beta}(\omega-1)^{\beta+1}(1-e^{2\pi i \beta})^{-1} \sum_{k=0}^{\infty} b_k(\omega-1)^k$ where $(\omega-1)^{\beta+1}$ is defined to be positive on the upper part of the cut $[1, \infty)$ and

$$b_k = \Gamma(\beta+1)(-1)^k \frac{\Gamma(k+1)}{\Gamma(\beta+k+2)} a_k \quad (34)$$

proving the statement when $\alpha = 0$. Using the second part of Lemma 20, the general case follows from it by integration by parts in the branch jump formula. An explicit example is shown in §6. \square

4.3 Singularity Elimination Theorem

Theorem 24 (Singularity Elimination). *Let Ω be a covering with fixed origin of $\mathbb{C} \setminus S$ where $0 \notin S$, assume F is analytic on Ω , that ω is on the boundary of Ω and that F has a singularity of type (1) at ω . Without loss of generality, we can assume that the projection of ω on \mathbb{C} is 1. Then the singularity can be eliminated by a combination of an appropriate L_β and a composition with a rational map such as those in (26).*

Proof of Theorem 24. The proof follows from Lemmas 19, 20, and items 1, 3 and 4 of Note 16 at the beginning of §4.1. \square

- Note 25** (Comments on Theorem 24). 1. Theorem 24 yields a practical method to apply simple convolution and conformal maps to make the local behavior near a singularity purely analytic. Since analyticity and singularity are highly sensitive to being distinguished numerically, this therefore provides a numerical mechanism to refine both the location of the singularity and also to refine the convolution parameter β , in order to determine the power exponent α which characterizes the nature of the original singularity. This is particularly useful when empirical analysis is the only option available. See examples in §6.
2. After eliminating a singularity (say at ω) of F , if we uniformize the Riemann surface of the new function F_1 , then $z = \psi(\omega) \in \mathbb{D}$, $F \circ \varphi$ is analytic at z and can be calculated convergently and with rigorous bounds. This means that the complete information about the singularity of F (such as the functions A, B if the singularity is of type (1)) follows. Uniformization of the new surface may be impractical, in which case an appropriate Conformal-Taylor expansion (see §5.3) would provide, with sub-optimal rate of convergence, the same information (or, non-rigorously, using Padé approximants).
3. In practical computations we noticed that the precision of the local information obtained from singularity elimination is usually significantly better than what is obtained numerically from an explicit uniformization map. See for example the Painlevé I computation described in Note 2.
4. There are important special cases in which all singularities are eliminated, for example arrays of pure singularities of the type $\sum_{k=0}^n (\omega - \omega_k)^\alpha$, which can be transformed by an appropriate L_β into a sum of logs, which becomes rational after differentiation.
5. Still for empirical analysis, for all three maps in (26) analytic continuation past 1 of φ^*F leads to the second Riemann sheet of F . For example, the map φ_0 takes the origin of the second Riemann sheet of F to $\omega = 2$ on the first Riemann sheet of φ_0^*F . Therefore, singularity elimination provides access to higher Riemann sheets. This will be an important element of the tools developed in §5 to refine approximate data about the Riemann surface.

Note 26 (Important special cases of singularity transformation and elimination). For example, we can manipulate and eliminate the log singularity at $\omega = 1$ of the elliptic integral function $\mathbb{K}(\omega)$. See §6.5.

4.4 The counterpart on series of the singularity elimination operator

Both steps of the analytic operations described above for singularity elimination have a simple and explicit counterpart as operations at the level of the series coefficients, taking Maclaurin polynomials to Maclaurin polynomials. This is important in applications, since series compositions with many coefficients is computer-algebra time-expensive. Recall first the explicit expression (27) for the action of the convolution operator L_β on series. Here we consider the second step, that of singularity elimination, and derive explicit formulas for the composition with the elimination maps φ_0 , φ_1 and φ_2 listed in equation (26) of item 3 of Note 16.

Lemma 27. *On the level of series, the operator φ_0^* of composition with the conformal map φ_0 is given by*

1. $\varphi_0^*(\sum_{k=1}^n a_k \omega^k) = \sum_{k=1}^n b_k \omega^k$ where

$$b_0 = a_0; \quad b_k = \sum_{l=0}^{\lfloor (k+1)/2 \rfloor} U_{k,l} a_l \quad (35)$$

where $U_{k,l}$ is the coefficient of x^l in the k th Chebyshev polynomial of the second kind $U_k(x)$, explicitly,

$$U_{k,l} = \begin{cases} (-1)^l 2^{2l+1} \binom{\frac{k+1}{2} + l}{\frac{k-1}{2} - l}, & k \text{ odd} \\ (-4)^l \binom{\frac{k}{2} + l}{\frac{k}{2} - l}, & k \text{ even} \end{cases} \quad (36)$$

2. φ_1^* acts by $\varphi_1^*(\sum_{k=1}^n a_k \omega^k) = \sum_{k=1}^n b_k \omega^k$ where

$$b_0 = a_0; \quad b_k = 4 \sum_{l=1}^k \tilde{U}_{k,l} a_l \quad (37)$$

where $\tilde{U}_{k,l}$ is the coefficient of x^l in the k th Chebyshev polynomial $U_k(2x - 1)$.

3. φ_2^* acts by $\varphi_2^*(\sum_{k=1}^n a_k \omega^k) = \sum_{k=1}^n b_k \omega^k$, where the new series coefficients b_k are related to the original series coefficients a_k via

$$b_0 = a_0; \quad b_k = 2 \sum_{l=0}^k U_{k,l} a_{2l+1}; \quad (k \text{ odd}), \text{ and } b_k = 2 \sum_{l=1}^k U_{k,l} a_{2l}; \quad (k \text{ even}) \quad (38)$$

Proof. We prove only part 3., since all three proofs are very similar. Define $f(\omega) = \frac{\omega}{2(1-x\omega)}$.

Then,

$$(\varphi_2^* f)(\omega) = \frac{\omega}{1-2x\omega+\omega^2} \quad (39)$$

which is, up to multiplication by ω , the known generating function of $U_k(x)$:

$$\sum_{k=0}^{\infty} U_k(x) \omega^k = \frac{1}{1-2x\omega+\omega^2}$$

and the rest follows easily by comparing coefficients. \square

Note 28 (Remarks on numerical accuracy). 1. Since the calculation of the b_k from the a_k involves summations, there can be cancellations, which could potentially become significant for large k . The following lemma addresses the question of the accuracy of the b_k , or even how many coefficients can be meaningfully retained. This is relevant also for selecting which map results in the minimal loss of accuracy. This is an interesting question for which examples will be given in an accompanying paper [28], and for which rigorous estimates are under investigation.

Lemma 29. For fixed large k , $|U_{k,l}|$ reaches its maximum value M_k at $l \sim \frac{1}{2\sqrt{2}}k + \frac{1}{8}(2\sqrt{2} - 5)$

$$M_k \sim \frac{2^{-1/4}}{\sqrt{\pi k}} (1 + \sqrt{2})^{k+1}, \quad k \rightarrow \infty$$

Proof. This result can be derived by asymptotically solving the equation $U_{k,l}/U_{k,l-1} = 1$ for $l = l(k)$, and using Stirling's formula for large k in $U_{k,l(k)}$. \square

For example, using φ_0^* , taking into account the position of the maximum, for large k the coefficient b_k involves cancellations of terms a_m , with $m \leq k$ weighted by $(1 + \sqrt{2})^{2m} \approx 6^m$.

2. In general, the accuracy needed can be calculated similarly, from the capacity C .

5 Probing empirically the Riemann surface. Quantitative analysis of known methods and various improvements.

In this Section we address the question of how to extrapolate the function F when the only input is a finite number n of terms of its Maclaurin series about some point. Evidently nothing rigorous can be said if n is fixed, and we focus on methods that are efficient and convergent as $n \rightarrow \infty$. We present methods to determine approximate information about the singularity structure of F , and methods to refine and corroborate this approximate information. We also adapt known results to provide precise rates of the convergence of these methods.

5.1 Overview of Padé approximation properties

Diagonal and near-diagonal Padé approximation is one of the most frequently used methods for empirical reconstruction.

Definition 30. The $[m/n]$ Padé approximant of F at $\omega = 0$ is the unique rational function A_m/B_n , with A_m a polynomial of degree at most m , and B_n a polynomial of degree at most n , for which we have

$$F(\omega) - \frac{A_m(\omega)}{B_n(\omega)} = \mathcal{O}(\omega^{m+n+1}), \quad \omega \rightarrow 0 \quad (40)$$

If we normalize $B_n(0) = 1$, then A_m and B_n are also unique. Since it can be calculated directly from the Maclaurin series M_F of F , we also say that $[m/n]$ is the Padé approximant of M_F .

A sequence of Padé approximants $\{[n/n]\}_{n \in \mathbb{N}}$ is called diagonal, and $\{[m_j/n_j]\}_{j \in \mathbb{N}}$ is near-diagonal if $n_j \rightarrow \infty$ and $m_j/n_j \rightarrow 1$ as $j \rightarrow \infty$.

In spite of their simplicity (they are rational functions with the same Maclaurin series as F , inasmuch as their degree permits) Padé approximants are, in most applications, uncannily accurate and able to detect poles and branch points in the whole complex domain (in principle).

However, except for special types of functions such as Riesz-Markov ones (see [73, 29] and references therein, and Note 31), they do not generally converge pointwise, but only in a weaker sense, in the sense of capacity theory. For this reason Padé approximants can only be used as an exploratory tool. Nevertheless, we will explain how these exploratory findings can be backed up rigorously, in the limit $n \rightarrow \infty$, see Note 34, part 3.

We briefly describe some important results (both negative and positive) concerning the convergence of Padé approximants, which seem to be little known to the applied community, outside the specialized literature. We also propose practical methods to overcome some of the limitations of Padé approximants, see Notes 34, parts 1 and 4.

An intrinsic limitation is immediately clear: as any sequence of rational approximations, they can only converge in some domain of single-valuedness of their associated function.

In fact, even for single-valued functions, uniform convergence of *some* diagonal Padé subsequence to general meromorphic functions, the Baker-Gammel-Wills conjecture [9], was settled in the negative in a remarkable paper of Lubinsky in 2003 [54]. The phenomenon that prevents pointwise convergence are the so-called spurious poles, or Froissart doublets, appearing at points unrelated to the properties of the associated function. In practice however, most often spurious poles appear infrequently and their exploratory value is largely unaffected.

Diagonal (and near-diagonal) Padé approximations do converge in a weaker sense, namely in capacity, and in this sense they “choose” a maximal domain of single-valuedness where they converge, maximizing also the rate of convergence near $\omega = 0$. This choice however also comes with a drawback: points of interest of F may be hidden in their boundary of convergence. This is actually a common occurrence in applications, and we propose methods to detect such hidden singularities: see Note 34.

5.2 Convergence of Padé approximants

Convergence in capacity is also a very difficult question, only elucidated in 1997, in the fundamental paper of Stahl [70]. It is interesting to note that convergence in capacity is established at this time only for functions analytic on Riemann surfaces which are **universal covers** of $\mathbb{C} \setminus E$, for sets E of zero logarithmic capacity or in domains in \mathbb{C} bounded by piecewise analytic arcs under a stringent symmetry condition [70]. We focus on the first type of functions, the only ones of interest here.

The general theory of Padé approximants summarized below is based on [70]. For further developments and refinements, see [6, 57].

The theory is best described by doing an inversion and **placing the point of expansion at infinity** rather than at $\omega = 0$. It is shown in [70] that there exists a domain $\mathcal{D} \subset \hat{\mathbb{C}}$, unique up to a capacity zero set, whose boundary has minimal logarithmic capacity, which contains ∞ and where F is analytic and single valued. This \mathcal{D} is the domain where near-diagonal Padé approximants converge in capacity to F . The rate of convergence is controlled by the Green’s function $g_{\mathcal{D}}$ (see, e.g., [72, 65, 67]) relative to infinity as follows. Define $G_{\mathcal{D}} = e^{-g_{\mathcal{D}}}$. We have $G_{\mathcal{D}} \in [0, 1)$ and $G_{\mathcal{D}} > 0$ on $\mathcal{D} \setminus \{\infty\}$ (in the case of interest, where $\text{cap}(\mathcal{D}) > 0$). Then, summarizing from Theorem 1 by Stahl [70],

1. For any $\varepsilon > 0$ and any compact set $V \subset \mathcal{D} \setminus \{\infty\}$ we have

$$\lim_{n \rightarrow \infty} \text{cap}\{\omega \in V | (F - [m_j/n_j])(\omega) > (G_{\mathcal{D}}(\omega) + \varepsilon)^{m_j+n_j}\} = 0 \quad (41)$$

2. If F has branch points, which occurs iff $G_{\mathcal{D}} \neq 0$, then for any compact set $V \subset \mathcal{D} \setminus \{\infty\}$ and any $0 < \varepsilon \leq \inf_{\omega \in V} G_{\mathcal{D}}(\omega)$ we have

$$\lim_{n \rightarrow \infty} \text{cap}\{\omega \in V | (F - [m_j/n_j])(\omega) < (G_{\mathcal{D}}(\omega) - \varepsilon)^{m_j+n_j}\} = 0 \quad (42)$$

Note 31. 1. In the rather generic case when \mathcal{D} is simply connected, then $G_{\mathcal{D}} = |\psi_{\infty}|$, where ψ_{∞} is a conformal map from \mathcal{D} to \mathbb{D} , with $\psi_{\infty}(\infty) = 0$. Comparing with Theorem 1, we note that if the maximal domain of analyticity of F happens to be this \mathcal{D} , then the leading order rate of convergence in capacity of Padé would be optimal.

2. When \mathcal{D} is simply connected, in view of 1. above and (41), we see that Padé effectively “creates its own conformal map” of a single-valuedness domain for F , \mathcal{D} , that can be recovered, in the limit $n \rightarrow \infty$, from the harmonic function $|G_{\mathcal{D}}|$, obtained by taking the n -th root of the convergence rate (41).
3. In very special cases, such as Riesz-Markov functions, under some further restrictions, the convergence of Padé approximants is uniform on compact sets (cf. [29] and references therein). A Riesz-Markov is a function that can be written in the form

$$F(\omega) = \int_a^b \frac{d\mu(x)}{x - \omega}$$

where μ is a positive measure. Riesz-Markov functions occur frequently in certain applications, but general functions cannot be brought to this form. For example, a common situation in applications, discussed in more detail in §6.3.2 below, is the situation of two complex conjugate singularities in \mathbb{C} . This is not a Riesz-Markov function, and Padé produces curved arcs of poles (see Figure 8) which do not relate to the properties of the function.

4. As mentioned, for more general functions, Padé approximants may place spurious poles (“Froissart doublets”) on sets of zero capacity, “random” pairs of a pole and a nearby zero, unrelated to the function they approximate.
5. The numerators and denominators of Padé approximants are orthogonal polynomials, in a generalized sense, along arcs in the complex domain, but therefore without a bona-fide Hilbert space structure. According to [70], this is the ultimate source of capacity-only convergence, and of the appearance of Froissart doublets.
6. If F has only isolated singularities on the universal cover of $\hat{\mathbb{C}}$ with finitely many punctures, then $\partial\mathcal{D}$ is a set of piecewise analytic arcs joining branch points of F , and some accessory points (similar to those of the Schwarz-Christoffel formula) associated with junctions of these analytic arcs. For an example see Figure 8. Padé represents actual poles of F by poles, and branch points by lines (either straight or curved arcs) where poles accumulate.

Note 32 (Potential Theory and Physical Interpretation of Padé Approximants). There is a remarkable and intuitively useful physical interpretation, which can be derived from [70, 67], of the domain \mathcal{D} and of the placement of poles of Padé.

1. Take any set \mathcal{D}' of single-valuedness of F and let $E' = \partial\mathcal{D}'$ be its boundary. Thinking of E' as an electrical conductor we place a unit charge on E' , and normalize the electrostatic potential $V(x, y) = V(\omega)$, $\omega = x + iy$ (always constant along a conductor) by $V(E') = 0$. Then the electrostatic capacitance of E' is $\text{cap}(E') = 1/V(\infty)$.

2. The domain boundary $E = \partial\mathcal{D}$ of the domain of convergence of Padé is obtained by deforming the shape (keeping the singularity locations fixed) of the conductor E' (defined in item 1 of this Note) until it has minimal capacity.
3. The equilibrium measure μ on E is the equilibrium density of charges on E in the setting above. As $j \rightarrow \infty$ the poles of the near diagonal Padé approximants place themselves (except for a set of zero capacity) close to E , and Dirac masses placed at these poles converge in measure to μ [70].
4. For $\omega \in \mathcal{D}$, we have $e^{-g_{\mathcal{D}}(\omega)} = |G_{\mathcal{D}}(\omega)| = e^{-V(\omega)}$.

5.3 Conformal-Taylor (CT) and Conformal-Padé (CP)

We compare the accuracy of two methods that have been used in the physics literature. While they have been used rather infrequently and without convergence analysis, they can be quite useful to reach points outside of \mathbb{D} . In the Conformal-Taylor (CT) method (as defined above in §2.1) a domain $\mathcal{D} \subset \mathbb{C}$ of analyticity of F is chosen, and then one proceeds as in Theorem 1, with \mathcal{D} in guise of Ω . The Conformal-Padé method (CP) [74, 14, 27] consists of applying Padé approximants to CT, which typically results in a significant increase in accuracy, at the price of having convergence in capacity only. Surprisingly, the CP method appears to have been used even less frequently than CT.

Note 33. 1. If the domain \mathcal{D} happens to be the maximal domain of analyticity, then of course, Theorem 1 shows that CT is optimal.

2. The error control of each of CT and CP approximation is obtained from the map ψ as in Theorem 1.
3. Also as a consequence of Theorem 1, CT can be improved by choosing a domain \mathcal{D} with $\text{cap}(\mathcal{D})$ as small as possible within the class of domains having explicit conformal maps ψ .
4. To expand the class of explicit maps, we note that one only needs a map $\varphi : \mathbb{D} \rightarrow \mathcal{D}$ which is **surjective** (at the price of a slower rate of reconstruction of F).

Note 34 (Some Improvements to Conformal-Taylor (CT) and Conformal-Padé (CP)).

1. (Detecting singularities hidden in the analytic arcs of poles of Padé).

This is not an unusual situation. All resurgent functions coming from differential equations have their singularities along half-lines starting from the origin, and symmetry reasons generally make those rays part of the capacitor. This is the case, for instance, for the *tritrinquée* Painlevé transcendents, P_I – P_V . In general the leading singularity is a branch-point, and, to ensure single-valuedness, Padé “creates” a cut, a curve from the point to infinity where poles accumulate, thereby obscuring any genuine singularities along such cuts. Two ways to detect such “hidden” singularities are described here. The simplest method is to place an artificial probe singularity near the arc. By the potential theory interpretation of Padé we know that this additional singularity will distort the minimal capacitor, but it cannot move the genuine singularities. This simple procedure can be implemented as follows: assume that J is an analytic arc of the Padé approximants of the function $F \in \mathcal{G}$. Define $F_1(\omega) = F(\omega) + (\omega - \omega_0)^\alpha$ where $\alpha \notin \mathbb{Z}$ (a negative power is typically more effective), and ω_0 is a point in the proximity of the arc J . Clearly, the Padé

approximants of F_1 determine the values of F as well, simply by subtracting out $(\omega - \omega_0)^\alpha$. The capacitor of F_1 is necessarily different from that of F , since the probe singularity ω_0 must be part of the new capacitor. Generically, the arc J moves when ω_0 is chosen near any point of J which is a point of analyticity of F . Evidently too, points in J which are branched singularities of F cannot move.

2. The second method consists of applying a form of CT. Any nontrivial conformal map of domains in \mathbb{C} will typically distort all the arcs of Padé, exposing hidden singularities, and possibly hiding ones that were visible before, and exposing domains that lie on the second Riemann sheet relative to the cut $\partial\mathcal{D}$ (\mathcal{D} being the domain of convergence of Padé).
3. In the large n limit, CT provides a **rigorous** way to check the information inferred from a Padé analysis. Indeed, conformally mapping a mistaken domain (or parts of a Riemann surface), results in singularities in \mathbb{D} , seen in an n -th root test of CT. This provides a practical method to refine the conjectured domain (for example by tuning the conjectured locations of the singularities) to remove these spurious singularities in \mathbb{D} .
4. The singularities of F that lie on the boundary $\partial\mathcal{D}$ are mapped onto the unit circle \mathbb{T} , the boundary of \mathbb{D} , and can therefore be resolved using a discrete Fourier transform of the properly normalized Maclaurin coefficients.

Note 35. Other numerical and analytic methods to enhance the accuracy of Padé approximants, for the purpose of discovering precise information about the Riemann surface of a function from its Maclaurin approximants, will be described in an applications paper [28].

6 Illustrative Examples

In this Section we present some examples that illustrate the effectiveness of the uniformizing maps, and the methods of singularity elimination.

6.1 Resurgent Functions

Écalle's resurgent functions [37] are ubiquitous as solutions of equations in analysis. This ubiquity is fundamentally due to the closure of the family of resurgent functions under virtually all operations used in solving analytic equations. A partial list of natural applications is the following: (i) solutions of generic systems of linear or nonlinear ODEs with meromorphic coefficients [19]; (ii) solutions of difference and q-difference equations [13, 64]; (iii) saddle point expansions in finite dimensional exponential integrals [11, 51, 30, 31]; (iv) solutions of special classes of PDEs [22, 23, 24, 25, 26]. There is also significant evidence, both numerical and analytic, for resurgent behavior in some *infinite-dimensional* physical systems, for example in quantum field theory, statistical field theory and string theory [75, 55, 42, 43, 3, 35, 36, 32, 4, 47, 51].

A resurgent function f possesses in its *Borel plane*, the plane of a properly normalized inverse Laplace transform F of f , a relatively simple Riemann surface, Ω with a fundamental group having a rich structure of relations, encoded in Écalle's alien derivations and bridge equations. The behavior of the Borel transform near its singularities determines asymptotic and global properties of the original function f . The Riemann surface Ω of the Borel transform function F is the universal cover of \mathbb{C} with a discrete set of punctures, typically equally spaced. The singularities of F are generically of the elementary form in (1). In this paper we only partially exploit this rich

algebraic structure provided by Écalle’s bridge equations. Further implications of this algebraic structure will be described in a future publication.

The Riemann surface of a resurgent function F , its precise form of singularities, as well as a priori bounds for F in Ω , are predetermined from the equation from which it originates. Consider, for example, a function F with an asymptotic series at infinity, and satisfying a generic N -th order system of linear or nonlinear ordinary differential equations with meromorphic coefficients (see [19] for precise conditions). After normalization of the variables, the system can be presented in the standard form, $y'(x) = \Lambda y + x^{-1}By + g(y; x)$, where Λ and B are diagonal matrices with constant coefficients, and g contains the higher order terms in the linearization, as well as the nonlinear terms. The data Λ and B from the linearized problem determines the basic Borel plane structure of the Borel transform function F : the Borel transform is analytic on the universal cover of $\hat{\mathbb{C}} \setminus \cup_{j \leq N} \lambda_j \mathbb{Z}$, and at zero, and the *nature* of the singularities λ_j is determined by B . Furthermore, the nature of the singularities at all integer multiples, $\cup_{j \leq N} \lambda_j \mathbb{Z}$, is determined by the ODE. These singularities are all of the form indicated in (1). Difference and q-difference equations of roughly the same form are also known to have resurgent solutions [13, 64], and similar comments and methods apply.

For certain PDEs, such as the time-periodic one-particle Schrödinger equation, $i\psi_t = (H_0 + V_1(x, t))\psi$, where $H_0 = -\Delta + V(x)$ is the time-independent part and V_1 is time-periodic, the Borel singularities Σ_B have the following structured form: a periodic array of typically square root branch points (see e.g. [26]; exceptions are long range potentials such as Coulomb, see [21]), originating from the bottom of the continuous spectrum of H_0 , and periodic arrays of poles, which come from the eigenvalues and resonances (“dressed states”) of H_0 [23]. The solution can be extrapolated using the techniques described in this paper, providing far superior approximation to the time evolution, as well as providing access to higher Riemann sheets. The uniformization and conformal mapping methods described here give a new numerical approach to this well known difficult problem. Similar methods apply to the heat equation, or the wave equation with potential.

Exponential integrals provide another important context for studying extrapolation and resurgent asymptotics. Consider functions defined as exponential integrals,

$$f(\hbar) = \int_{\Gamma} e^{-g(x)/\hbar} d^n x$$

where f is a holomorphic function on an n -dimensional complex manifold, and Γ is a steepest descent integration cycle. In the Borel plane, there are isolated singularities at $g(x_c)$, associated with the critical points x_c of the exponent function. The critical points x_c can be classified according to their Arnold normal forms [7], and their location and hessian determine the building blocks from which a full trans-series expansion of f may be generated. The methods presented in this paper provide substantial improvements to extrapolations of formal expansions of such functions.

6.2 Painlevé equations PI-PV

The *tritonquée* Painlevé transcendents are resurgent functions. The Painlevé equations, P_I - P_V , have a common and simple Borel singularity structure, which can be arranged as integer-spaced singularities along the real line (excluding the origin). Even the Conformal-Padé method, based on the simple two-cut conformal map in (13), leads to a remarkably accurate extrapolation of the formal solution generated at infinity, throughout the complex plane: see [27] for a detailed analysis of the *tritonquée* solution of P_I . But with the Painlevé uniformizing maps of section §3.1

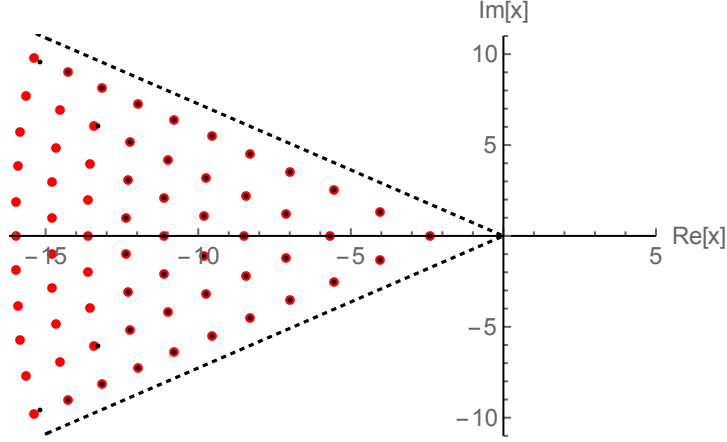


Figure 6: The poles of the *tritronquée* solution of the Painlevé 1 equation, which lie only in the wedge $\frac{4\pi}{5} \leq \arg(x) \leq \frac{6\pi}{5}$ of the complex plane, obtained by extrapolation of the asymptotic expansion about $x \rightarrow +\infty$, using 200 input coefficients. The smaller black dots show the results using the Conformal-Padé method in the Borel plane, as described in [27], while the larger red dots are obtained by replacing the conformal map with the Painlevé uniformizing map in Theorem 9. With exactly the same input data, the uniformizing map leads to a significantly better extrapolation. There is comparable accuracy throughout the domain of analyticity, $|\arg(x)| \leq \frac{4\pi}{5}$.

significantly better extrapolation can be achieved. For example, as mentioned already in Note 11, the Stokes constant (which is known analytically from isomonodromy [49] and from asymptotics [19]) can be determined numerically to extraordinary precision with surprisingly little input data [27].

A much stronger demonstration of the power of the uniformization map is to reconstruct the P_I *tritronquée* solution throughout its domain of analyticity, and in its pole sector $\frac{4\pi}{5} \leq \arg(x) \leq \frac{6\pi}{5}$, using only input from its asymptotic expansion about the opposite direction, as $x \rightarrow +\infty$. Recall that the solution of the P_I equation, $y''(x) = 6y^2 - x$, is meromorphic throughout the complex plane, and the special *tritronquée* solution has poles only in the wedge, $\frac{4\pi}{5} \leq \arg(x) \leq \frac{6\pi}{5}$ [33, 18]. Figure 6 shows as black dots 44 P_I *tritronquée* poles found using our Conformal-Padé approach of [27], starting with 200 terms of the asymptotic expansion generated at $x \rightarrow +\infty$, while the red dots show the first 66 P_I *tritronquée* poles found simply by adapting the analysis of [27] to use the uniformizing map in Theorem 9 instead of the conformal map in (13), and with exactly the same input data. The gain in precision in the pole sector, and also throughout the domain of analyticity, is quite dramatic. These numerical poles, even the first few ones, fit very precisely the asymptotic Boutroux structure [49, 27].

In addition, the uniformized extrapolation yields high-precision fine structure of the pole region. In the vicinity of a moveable pole, any P_I solution $y(x)$ has a Laurent expansion of the following form

$$\begin{aligned}
 y(x) \approx & \frac{1}{(x - x_{\text{pole}})^2} + \frac{x_{\text{pole}}}{10}(x - x_{\text{pole}})^2 + \frac{1}{6}(x - x_{\text{pole}})^3 + h_{\text{pole}}(x - x_{\text{pole}})^4 \\
 & + \frac{x_{\text{pole}}^2}{300}(x - x_{\text{pole}})^6 + \frac{x_{\text{pole}}}{150}(x - x_{\text{pole}})^7 + \dots
 \end{aligned} \tag{43}$$

All higher coefficients of this expansion are expressed as polynomials in the two parameters x_{pole} and h_{pole} . Thus, any P_I solution $y(x)$ is completely determined by two constants, x_{pole} and

h_{pole} , in the vicinity of any one of its poles. It is natural to characterize the *tritrinquée* solution by the two constants, x_{pole} and h_{pole} , at the closest pole to the origin. From the uniformized map extrapolation, we obtain the following high-precision values at this first pole:

$$x_1 = -2.38416876956881663929914585244876719041040881473785051267725... \quad (44)$$

$$h_1 = 0.0621357392261776408964901416400624601977407713738296636635333... \quad (45)$$

These are significantly higher precision than existing values. Furthermore, it is straightforward to optimize these values, to obtain even higher precision, if desired. Similar methods apply to the other Painlevé *tritrinquée* solutions, providing new methods to obtain high-precision computations for the Painlevé project [62], and also to compute high-precision spectral properties of certain Schrödinger operators [58, 60].

6.3 Improvement of Uniformization over Padé and Conformal-Padé (CP)

The generic improvement of analytic continuations based on uniformization maps, compared with other common methods such as Padé or Conformal-Padé (CP) [as illustrated in the previous section], can often be traced to some elementary properties of these maps, especially near the singularities. Here we illustrate this with some examples.

6.3.1 One Cut Complex Plane

For $\Omega = \mathbb{C} \setminus [1, \infty)$, the conformal map is in (12), and the uniformizing map of $\hat{\mathbb{C}} \setminus \{1, \infty\}$ is $\omega = 1 - e^{-z}$, with inverse $z = -\log(1 - \omega)$. The uniformizing map pushes the singularity at $\omega = 1$ to $z = \infty$. A Padé approximant of the truncated composed map $F \circ \varphi$, with either the conformal map or the uniformizing map, each mapped back to Ω , produces dramatically improved extrapolations throughout Ω . For example, for the one-branch-cut function $F(\omega) = (1 - \omega)^{-1/5}$, beginning with just 10 terms of a Maclaurin expansion at $\omega = 0$, Figure 7 shows the ratio of the extrapolated to the exact function, as the singularity is approached: $\omega \rightarrow 1^-$. The uniformization map is vastly superior. This is due to the typical exponential distortion of distance near the singularity. Ordinary Padé, without composition with either map, is not at all competitive.

6.3.2 Two Cut Complex Plane

Another common case in applications is the two-cut complex plane, $\Omega = \mathbb{C} \setminus (-\infty, -1] \cup [1, \infty)$. The conformal and uniformizing maps are given in (13) and (14), respectively, in §3. For example, applying this to the two-branch-cut function $F(\omega) = (1 - \omega^2)^{-1/5}$, with branch points at $\omega = \pm 1$, produces similar improvements as in §6.3.1. In this case the conformal map sends the cut ω plane to the interior of the unit disk in the z plane, while the uniformizing map sends the cut ω plane to the interior of the symmetric geodesic quadrilateral with boundaries given by orthogonal circles intersecting the unit disk at $z = \pm 1, \pm i$. See the left plot in Figure 2.

Even when these are not the exact conformal or uniformizing maps, such as in nonlinear problems where the singularities at $\omega = \pm 1$ are only the leading ones, generally repeated at all non-zero integers, the use of these two-cut maps leads to dramatic improvements, especially in the vicinity of these leading singularities [27]. This example is particularly relevant in applications, as there are many examples where the (Borel) singularities appear in integer multiples along oppositely directed straight lines: for example, all the *tritrinquée* Painlevé I-V solutions,

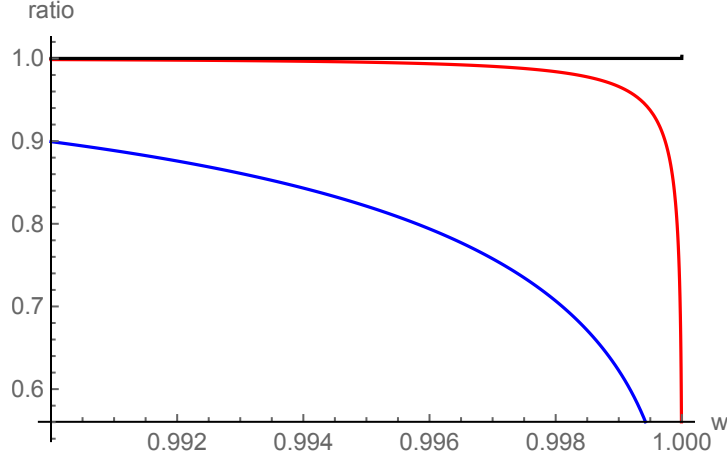


Figure 7: Ratio of the approximate to the exact one-branch-cut function $F(\omega) = (1 - \omega)^{-1/5}$, for a Padé approximation [blue], a Padé-Conformal approximation [red], and a Padé-Uniformized approximation [black]. Note the dramatically superior behavior of the uniformized approximation as the singularity is approached. These approximations are each generated starting with just 10 input coefficients of the series expansion of $F(\omega)$ at $\omega = 0$.

the Euler-Heisenberg effective action [34], and renormalon singularities in quantum field theory [10]. Another important configuration for applications consists of two complex conjugate

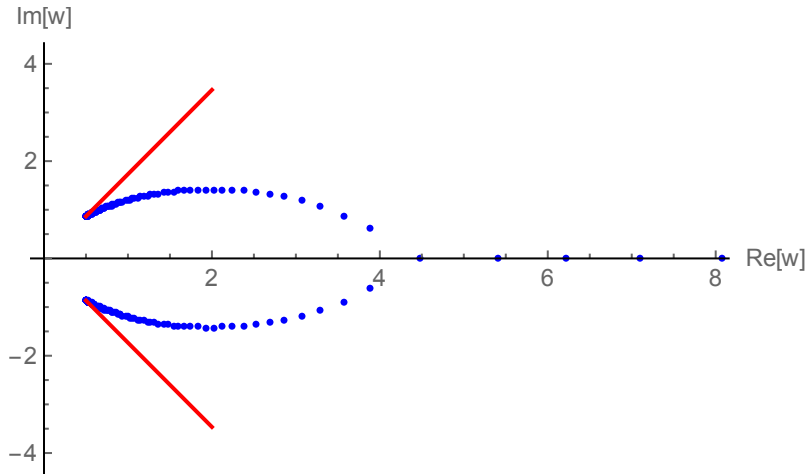


Figure 8: Arcs of Padé poles [blue points] for a pair of complex conjugate singularities, here at $\omega = e^{\pm i\pi/3}$, for the function $F(\omega) = (1 - 2\omega \cos(\pi/3) + \omega^2)^{-1/5}$. Padé generates arcs of poles, including unphysical poles on the positive real axis, while the natural radial cuts [red lines] are associated with the conformal map (46).

singularities at $\omega = e^{\pm i\theta}$. This type of configuration occurs in physical applications involving symmetry breaking [71, 12, 66, 69], and in differential equations arising in holographic models [41]. In this case, without a conformal or uniformizing map, Padé produces curved arcs of poles (see Figure 8) as well as artificial poles along the positive real axis. Problems due to these artificial poles can be mitigated by using a conformal or uniformizing map. The conformal map for this configuration is

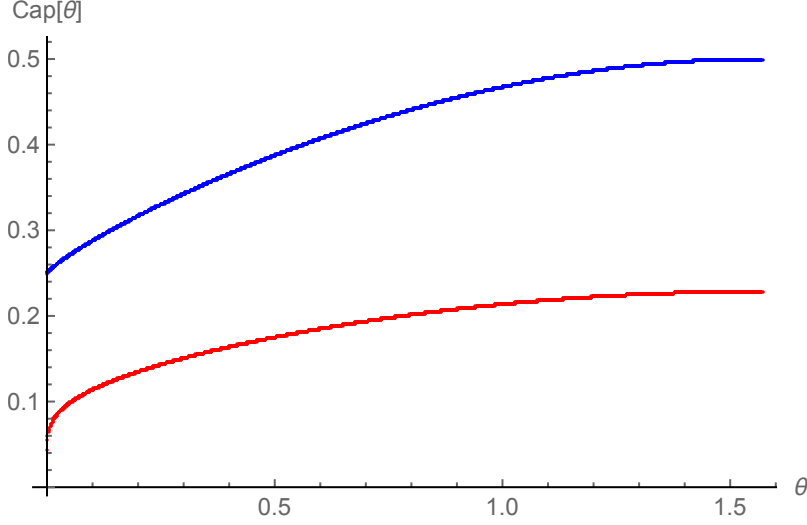


Figure 9: Capacity plot, showing $C_{\text{conf.}}(\theta)$ [blue curve] and $C_{\text{unif.}}(\theta)$ [red curve] from (47) and (48), respectively, as a function of $\theta \in [0, \pi/2]$, for the configuration with two complex conjugate singularities at $e^{\pm i\theta}$. Lower capacity corresponds to a superior extrapolation. The ratio of capacities gives the improvement of the geometric rate of convergence.

$$\omega = c(\theta) \frac{z}{(1+z)^2} \left(\frac{1+z}{1-z} \right)^{2\theta/\pi}, \quad c(\theta) = 4 \left(\frac{\theta}{\pi} \right)^{\theta/\pi} \left(1 - \frac{\theta}{\pi} \right)^{1-\theta/\pi} \quad (46)$$

and the uniformizing map is given by (15). The capacity factor for the two cases are

$$\text{conformal :} \quad C_{\text{conf.}}(\theta) = \frac{1}{4} \left(\frac{\theta}{\pi} \right)^{-\frac{\theta}{\pi}} \left(1 - \frac{\theta}{\pi} \right)^{\frac{\theta}{\pi}-1} \quad (47)$$

$$\text{uniformizing :} \quad C_{\text{unif.}}(\theta) = \frac{i \frac{\pi}{2} \sin \theta}{(\mathbb{K}(\frac{1}{2} + \frac{i}{2} \cot \theta))^2 + (\mathbb{K}(\frac{1}{2} - \frac{i}{2} \cot \theta))^2} \quad (48)$$

As shown in Figure 9, the uniformizing map has lower capacity, indicating a superior extrapolation. The uniformizing map has lower capacity, for all θ , and also has an explicit inversion. The conformal map is a simpler elementary function, but has no explicit inversion except for a few special cases of rational θ/π . A simple Padé approximation, which produces the minimal capacitor (for which there exist implicit transcendental expressions for the capacity [52, 46]), is inferior to both the conformal and uniformizing maps.

6.4 Further Discussion of some Uniformization Maps and Approximate Uniformization by Composition of Elementary Maps

With the exact uniformizing map, one can then analytically continue beyond the Riemann sheet, in principle onto all higher sheets. But even without the exact map, some degree of analytic continuation onto higher sheets can be achieved using approximate maps. (Access to higher Riemann sheets can also be achieved using singularity elimination (see §4 and §6.5). Consider the uniformization of the universal cover Ω of $\hat{\mathbb{C}} \setminus \{-1, 1, \infty\}$. This is achieved exactly by the map in (14). See Figure 2. The points A, B, C are mapped to $\{-1, \infty, 1\}$. The gray geodesic triangle in the Poincaré disk is conformally mapped by φ onto the upper half plane, and successive Schwarz

reflections across their circular sides continue φ to the whole disk, with image onto Ω (see [2], p. 379). Thus, the exact uniformization map permits systematic analytic continuation to higher Riemann sheets. The union of all reflected triangles is the unit disk \mathbb{D} . The image through φ of a curve in \mathbb{D} crossing a reflection of $(A, B), (B, C), (C, A)$ crosses the real line between $(-\infty, -1), (1, \infty), (-1, 1)$ resp. The collection, modulo homotopies, of images through φ of all the curves in \mathbb{D} (each of them traceable using this geometric description) represents the universal covering of $\hat{\mathbb{C}} \setminus \{-1, 1, \infty\}$.

In the left figure of Figure 2, the blue path inside the disk is mapped to the spiral path in the middle figure on the universal cover Ω of $\mathbb{C} \setminus \{-1, 1\}$. The improvement of the rate of convergence is determined by the conformal distance to the boundary of the unit disk, and is $\sim 0.228^n$ near zero, and the rate is about 0.83^n at the other end of the spiral.

However, even without the *exact* uniformization map, an accurate *approximate* uniformization of the same universal cover can be achieved by the following iterative application of elementary conformal maps. We apply the construction of iterated maps in Theorem 12. The conformal map $z = \psi_n(z)$ from Theorem 12 maps a surface with n symmetric radial cuts to the unit disk. Applying ψ_2 to $\hat{\mathbb{C}} \setminus \{-1, 1, \infty\}$ produces 4 symmetric cuts emanating from $\pm 1, \pm i$. Subsequent application of ψ_4 produces 8 symmetric cuts emanating from $e^{2\pi ij/8}, j = 0, \dots, 7$. Each of these maps is an elementary conformal map. Theorem 12 implies that iterating this to all orders, we obtain a full uniformization of the universal cover Ω of $\hat{\mathbb{C}} \setminus \{-1, 1, \infty\}$. But even a *finite* iteration of this procedure permits an accurate extrapolation and analytic continuation onto higher sheets of Ω , all in terms of elementary conformal maps. For example, in the center plot of Figure 2, the spiral path is the image of the blue path in the left plot, through the exact uniformizing map, but it is also the image of the blue curve on the right, through the elementary map $\varphi_2 \circ \dots \circ \varphi_{2^n}$, iterated up to $n = 6$. The rate of improvement is $\sim 0.255^n$ near zero and $\sim 0.91^n$, at the end, which are comparable to the exact uniformization results quoted above.

6.5 Singularity Elimination Example

In this section we illustrate the general procedure of singularity elimination by using a suitable convolution operator L_β in (24) to transform the logarithmic singularity of the elliptic integral function $\mathbb{K}(\omega)$ into a square root singularity, and then eliminating this singularity by composition with a suitable conformal map. We choose this example because of its practical interest and also because we can compare the general expressions in §4 with analytic results for the transformation of hypergeometric functions. We define

$$F(\omega) = \mathbb{K}(\omega) = \frac{\pi}{2} {}_2F_1\left(\frac{1}{2}, \frac{1}{2}, 1; \omega\right) \quad (49)$$

The expansions as $\omega \rightarrow 0^+$ and $\omega \rightarrow 1^-$ are:

$$F(\omega) \sim \frac{1}{2} \sum_{k=0}^{\infty} \left(\frac{\Gamma(k + \frac{1}{2})}{\Gamma(k + 1)} \right)^2 \omega^k \quad , \quad \omega \rightarrow 0^+ \quad (50)$$

$$F(\omega) \sim A(\omega) \ln(1 - \omega) + B(\omega) \quad , \quad \omega \rightarrow 1^- \quad (51)$$

where at the logarithmic singularity the regular functions $A(\omega)$ and $B(\omega)$ behave as

$$A(\omega) = -\frac{1}{\pi} \mathbb{K}(1-\omega) = -\frac{1}{\pi} \sum_{k=0}^{\infty} \left(\frac{\Gamma(k+\frac{1}{2})}{\Gamma(k+1)} \right)^2 (1-\omega)^k, \quad \omega \rightarrow 1^- \quad (52)$$

$$B(\omega) = -\sum_{k=0}^{\infty} \left(\frac{\Gamma(k+\frac{1}{2})}{\Gamma(k+1)} \right)^2 \left(\psi\left(k+\frac{1}{2}\right) - \psi(k+1) \right) (1-\omega)^k, \quad \omega \rightarrow 1^- \quad (53)$$

The convolution operator (24), with $\beta \notin \mathbb{Z}$, acting on F leads to

$$(L_{\beta}F)(\omega) = \frac{\pi}{2(1+\beta)} \omega {}_2F_1\left(\frac{1}{2}, \frac{1}{2}, 2+\beta; \omega\right) \quad (54)$$

$$= \frac{\Gamma(1+\beta)}{2} \sum_{k=0}^{\infty} \frac{\Gamma(k+\frac{1}{2})^2}{\Gamma(k+1)\Gamma(2+k+\beta)} \omega^{k+1}, \quad \omega \rightarrow 0^+ \quad (55)$$

$$\sim \tilde{A}(\omega)(1-\omega)^{1+\beta} + \tilde{B}(\omega), \quad \omega \rightarrow 1^- \quad (56)$$

where $\tilde{A}(\omega)$ and $\tilde{B}(\omega)$ are analytic at $\omega = 1$. Equation (55) confirms the general expression (27) relating the original expansion coefficients of $F(\omega)$ with those of the convolved function $(L_{\beta}F)(\omega)$. To transform the original logarithmic singularity at $\omega = 1$ to a square root behavior at $\omega = 1$ we choose $\beta = -\frac{1}{2}$, to obtain

$$(L_{-\frac{1}{2}}F)(\omega) = \pi \omega {}_2F_1\left(\frac{1}{2}, \frac{1}{2}, \frac{3}{2}; \omega\right) = \pi \sqrt{\omega} \arcsin(\sqrt{\omega}) \quad (57)$$

(Of course, in this special case composition with the series of \sin^2 results in factorial convergence of the composed series, far superior to the generic rate in the optimality theorem.)

$L_{\beta}F$ is analytic at zero and singular at $\{1, \infty\}$, and at $\{0, 1, \infty\}$ on higher Riemann sheets. Its Maclaurin series is

$$\frac{\sqrt{\pi}}{4} \sum_{k=0}^{\infty} \frac{\Gamma(k+\frac{1}{2})^2}{\Gamma(k+1)\Gamma(k+\frac{3}{2})} \omega^{k+1}, \quad \omega \in \mathbb{D} \quad (58)$$

and its singularity structure near $\omega = 1$ is

$$\tilde{A}(\omega)(1-\omega)^{1/2} + \tilde{B}(\omega) \quad (59)$$

where

$$\tilde{A}(\omega) = -\pi \sqrt{\omega} \frac{\arcsin(\sqrt{1-\omega})}{\sqrt{1-\omega}} = -\frac{\pi}{2} \sqrt{\omega} \sum_{k=0}^{\infty} (-1)^k \frac{\Gamma(k+\frac{1}{2})^2}{\Gamma(k+1)\Gamma(k+\frac{3}{2})} (1-\omega)^k \quad (60)$$

$$\tilde{B}(\omega) = \frac{\pi^2}{2} \sqrt{\omega} \quad (61)$$

We see from (60) that the expansion coefficients of $\tilde{A}(\omega)$, the function in (59) multiplying the square root behavior, match the general expression in (34). In the practical situation where we only have (a finite number of) the original expansion coefficients, we simply transform the expansion coefficients according to the convolution results in §4.4.

The final step of the singularity elimination is to make a composition map that transforms the square root behavior in (59) into analytic behavior, using the map φ_2 in (26). The Riemann

surface of the new function, after composition with $z \mapsto iz$ is uniformized by (18) which brings the original singular point -1 inside the unit disk, where (assuming we did not know \tilde{A}, \tilde{B}) these could be calculated with extremely high accuracy.

A similar comparison can be made for a general hypergeometric function

$$F(\omega) = {}_2F_1(a, b, c; \omega) \quad (62)$$

$$\sim A(\omega)(1-\omega)^{c-a-b} + B(\omega) \quad , \quad \omega \rightarrow 1^- \quad (63)$$

for which the convolved function becomes a generalized hypergeometric function with a different singularity exponent at $\omega = 1$:

$$(L_\beta F)(\omega) = \frac{1}{(1+\beta)\Gamma(1+\beta)} \omega {}_3F_2(1, a, b, c, 2+\beta; \omega) \quad (64)$$

$$\sim \tilde{A}(\omega)(1-\omega)^{c-a-b+1+\beta} + \tilde{B}(\omega) \quad , \quad \omega \rightarrow 1^- \quad (65)$$

For a given original singularity exponent, $c - a - b$, a suitable choice of β transforms the singularity into a square root singularity, which can then be eliminated by composition with one of the conformal maps in (26).

7 Appendix: some useful conformal maps

Here we record a few examples of conformal maps in frequently encountered cases of resurgent functions, and which can also serve as guides in more complicated arrangements of singularities. General conformal maps can in principle be derived from Schwarz-Christoffel, as described below, but this procedure is rather tedious, and in cases of symmetry the resulting maps can be quite elementary. For a comprehensive list of known conformal maps, see [50].

The maps φ_1 and φ_2 in (26) take \mathbb{D} to $\mathbb{C} \setminus [1, \infty)$ and $\mathbb{C} \setminus (-\infty, -1] \cup [1, \infty)$, respectively. The latter case generalizes to two more general cuts on the real line, $\mathbb{C} \setminus (-\infty, -a] \cup [b, \infty)$ with $a, b \in \mathbb{R}^+$, for which

$$\omega = \varphi_{ab}(z) = \frac{4abz}{a(1+z)^2 + b(1-z)^2} \quad \leftrightarrow \quad z = \frac{1 - \sqrt{\frac{a(b-\omega)}{b(a+\omega)}}}{1 + \sqrt{\frac{a(b-\omega)}{b(a+\omega)}}} \quad (66)$$

For a symmetric set of n singularities on the unit circle, $\mathbb{C} \setminus \bigcup_{j=0}^{n-1} e^{2\pi ij/n} [1, \infty)$, the conformal map producing symmetric radial cuts is

$$\omega = \varphi_n(z) = \frac{2^{2/n} z}{(1+z^n)^{2/n}} \quad (67)$$

used in §3.2. For two complex conjugate radial cuts, $\mathbb{C} \setminus e^{i\theta} [1, \infty) \cup e^{-i\theta} [1, \infty)$, the conformal map is as in (46), and this extends to a symmetric set of n such paired cuts as:

$$z = \varphi_{n,\theta}(z) = c_n(\theta) \frac{z}{(1+z^n)^{2/n}} \left(\frac{1+z^n}{1-z^n} \right)^{2\theta/\pi} \quad , \quad c_n(\theta) = 2^{2/n} \left(\frac{n\theta}{\pi} \right)^{\theta/\pi} \left(1 - \frac{n\theta}{\pi} \right)^{1/n-\theta/\pi} \quad (68)$$

For a general finite set of branch points, Padé produces a conformal map in the infinite order limit, and this map corresponds to the minimal capacitor. Recall the discussion in §5. The analytic description of this minimal capacitor conformal map is as follows [46]. Let $S = \{\omega_1, \dots, \omega_n\}$ be

branch points, and \mathcal{C} the minimal capacitor, with the point of analyticity placed at infinity. The conformal map φ that takes $\mathbb{C} \setminus \mathbb{D}$ to $\mathbb{C} \setminus \mathcal{C}$, with $+\infty \mapsto +\infty$, has the Taylor expansion at infinity

$$\varphi(\zeta) = C_B \zeta + \sum_{k=0}^{\infty} b_k \zeta^{-k} \quad (69)$$

where C_B is the capacity. There is a set $\{a_1, \dots, a_{n-2}\} \subset \mathcal{C}$ of auxiliary parameters such that φ satisfies the equation

$$\log \zeta = \int^{\varphi(\zeta)} \sqrt{\frac{\prod_{j=1}^{n-2} (s - a_j)}{\prod_{j=1}^n (s - \omega_j)}} ds \quad (70)$$

These auxiliary parameters are the intersection points of the set of analytic arcs of \mathcal{C} , the limiting location set of the poles of the diagonal Padé approximation $P_n[F]$ for any function F having S as the set of branch points, and being analytic in the complement of \mathcal{C} . (For example, in the infinite n limit, in Figure 8 the point on the positive real axis near $\omega \approx 4.5$ would tend to the single intersection point for this configuration.) The analytic arcs γ_j (γ'_j , resp) joining a_1 with ω_j , $j = 1, \dots, n-1$ (a_1 to a_j , $j = 2, \dots, n-2$, resp.) are given by

$$\Re \int_{\gamma_k}^{\omega} \sqrt{\frac{\prod_{j=1}^{n-2} (s - a_j)}{\prod_{j=1}^n (s - \omega_j)}} ds = 0 \quad \text{and} \quad \Re \int_{\gamma'_m}^{\omega} \sqrt{\frac{\prod_{j=1}^{n-2} (s - a_j)}{\prod_{j=1}^n (s - \omega_j)}} ds = 0 \quad (71)$$

where $k = 1, \dots, n-1$ and $m = 2, \dots, n-2$. In cases of symmetrically distributed branch points, these integrals can be expressed in terms of elementary or elliptic functions [52], and in more general cases the minimal capacitor produced by Padé can be found numerically [46]. This construction benefits from physical intuition arising from the interpretation of the minimal capacitor in terms of potential theory (see §5).

Acknowledgements

We thank R. Costin for numerous helpful discussions and comments. This work is supported in part by the U.S. Department of Energy, Office of High Energy Physics, Award DE-SC0010339.

References

- [1] W. Abikoff, The Uniformization Theorem, The American Mathematical Monthly, v. 88, No. 8, pp. 574–592 (1981).
- [2] M. J. Ablowitz and A. S. Fokas, Complex variables, 2nd. ed., Cambridge University Press (2003).
- [3] I. Aniceto, R. Schiappa and M. Vonk, “The Resurgence of Instantons in String Theory,” Commun. Num. Theor. Phys. **6**, 339 (2012), [arXiv:1106.5922](https://arxiv.org/abs/1106.5922).
- [4] I. Aniceto, “The Resurgence of the Cusp Anomalous Dimension,” J. Phys. A **49**, 065403 (2016), [arXiv:1506.03388](https://arxiv.org/abs/1506.03388).
- [5] I. Aniceto, G. Basar and R. Schiappa, “A Primer on Resurgent Transseries and Their Asymptotics,” Phys. Rept. **809**, 1 (2019), [arXiv:1802.10441](https://arxiv.org/abs/1802.10441).
- [6] A. Aptekarev and M. L. Yattselev, Padé approximants for functions with branch points – strong asymptotics of Nuttall–Stahl polynomials, Acta Math. **215**, 217–280 (2015).

- [7] V. I. Arnold, S. M. Gusein-Zade, A. N. Varchenko, *Singularities of Differentiable Maps (Monodromy and Asymptotics of Integrals)* (Birkhauser, Berlin 1988).
- [8] G. A. Baker, and P. Graves-Morris, *Padé Approximants*, (Cambridge University Press, 2009).
- [9] G. A. Baker, J. L. Gammel, and J. G. Wills, An investigation of the applicability of the Padé approximant method, *J. Math. Anal. Appl.* **2**, 405–418. (1961).
- [10] M. Beneke, “Renormalons,” *Phys. Rept.* **317**, 1-142 (1999), [arXiv:hep-ph/9807443](#).
- [11] M. V. Berry, C. Howls, Hyperasymptotics, *Proc. Roy. Soc. Lond A*, **430**, 653-668 (1990); Hyperasymptotics for integrals with saddles, *Proc. Roy. Soc. A*, **434**, 657-675 (1991).
- [12] C. Bertrand, S. Florens, O. Parcollet, and X. Waintal, “Reconstructing Nonequilibrium Regimes of Quantum Many-Body Systems from the Analytical Structure of Perturbative Expansions”, *Phys. Rev. X* **9**, 041008 (2019), [arXiv:1903.11646](#).
- [13] B. L. J. Braaksma, Transseries for a class of nonlinear difference equations, *J. Difference Eq. and Appl.*, **5**, (2001).
- [14] E. Caliceti, M. Meyer-Hermann, P. Ribeca, A. Surzhykov and U. D. Jentschura, “From useful algorithms for slowly convergent series to physical predictions based on divergent perturbative expansions,” *Phys. Rept.* **446**, 1 (2007), [arXiv:0707.1596](#).
- [15] Cannon, J.W., Dicks, W. On hyperbolic once-punctured-torus bundles II: fractal tessellations of the plane. *Geom Dedicata* **123**, 11–63 (2006).
- [16] I. Caprini, J. Fischer, G. Abbas and B. Ananthanarayan, “Perturbative Expansions in QCD Improved by Conformal Mappings of the Borel Plane,” in *Perturbation Theory: Advances in Research and Applications*, (Nova Science Publishers, 2018), [arXiv:1711.04445](#).
- [17] Costin, O.; Costin, R. D.; Huang, M. Tronquée solutions of the Painlevé equation PI. *Constr. Approx.* **41** (2015), no. 3, 467–494.
- [18] Costin, O.; Huang, M.; Tanveer, S. Proof of the Dubrovin conjecture and analysis of the tritronquée solutions of PI. *Duke Math. J.* **163** (2014), no. 4, 665–704.
- [19] O. Costin, On Borel Summation and Stokes Phenomena for Rank-1 Nonlinear Systems of Ordinary Differential Equations, *Duke Math. J.*, **93**, no. 2, 289-344 (1998).
- [20] O. Costin, *Asymptotics and Borel summability*, (Chapman and Hall/CRC, 2008).
- [21] Costin, O.; Lebowitz, J. L.; Tanveer, S. Ionization of Coulomb systems in \mathbb{R}^3 by time periodic forcings of arbitrary size. *Comm. Math. Phys.* **296** (2010), no. 3, 681–738.
- [22] O. Costin and S. Tanveer, Nonlinear evolution PDEs in $\mathbb{R}^+ \times \mathbb{C}^d$: existence and uniqueness of solutions, asymptotic and Borel summability properties. *Ann. Inst. H. Poincaré Anal. Non Linéaire*, **24**, 795-823 (2007).
- [23] O. Costin, M. Huang, Gamow vectors and Borel summability in a class of quantum systems. *J. Stat. Phys.* **144**, no. 4., 846-871 (2011).
- [24] Costin O.; Luo, G.; Tanveer, S. Integral formulation of 3D Navier-Stokes and longer time existence of smooth solutions. *Commun. Contemp. Math.* **13** (2011), no. 3, 407–462.

- [25] Costin, O.; Park, H.; Takei, Y. Borel summability of the heat equation with variable coefficients. *J. Differential Equations* 252 (2012), no. 4, 3076–3092.
- [26] Costin, Ovidiu; Costin, Rodica D.; Lebowitz, J.L.; Nonperturbative time dependent solution of a simple ionization model, *Comm. Math. Phys.* 361 (2018), no. 1, 217–238, (2018).
- [27] O. Costin and G. V. Dunne, “Resurgent extrapolation: rebuilding a function from asymptotic data. Painlevé I,” *J. Phys. A* 52, no. 44, 445205 (2019), [arXiv:1904.11593](#).
- [28] O. Costin and G. V. Dunne, to appear.
- [29] D. Damanik and B. Simon, Jost functions and Jost solutions for Jacobi matrices, I. A necessary and sufficient condition for Szegő asymptotics, *Invent. Math.* 165, 1-50 (2006).
- [30] E. Delabaere and F. Pham, “Resurgent Methods in Semiclassical Asymptotics”, *Ann. de l’I. Henri Poincaré*, 71, 1-94 (1999).
- [31] E. Delabaere and C. Howls, Global asymptotics for multiple integrals with boundaries, *Duke Math. J.*, v. 112, 199-264 (2002).
- [32] D. Dorigoni and Y. Hatsuda, “Resurgence of the Cusp Anomalous Dimension,” *JHEP* 1509, 138 (2015), [arXiv:1506.03763](#).
- [33] B. Dubrovin, T. Grava, and C. Klein, “On universality of critical behavior in the focusing nonlinear Schrödinger equation, elliptic umbilic catastrophe and the tritronquée solution to the Painlevé-I equation”, *J. Nonlinear Sci.* 19, 57-94 (2009).
- [34] G. V. Dunne, “Heisenberg-Euler effective Lagrangians: Basics and extensions,” in *From fields to strings*, vol. 1, 445-522, M. Shifman et al (eds.) et al, (World Scientific, Singapore, 2005), [arXiv:hep-th/0406216](#).
- [35] G. V. Dunne and M. Ünsal, “Resurgence and Trans-series in Quantum Field Theory: The CP(N-1) Model,” *JHEP* 11, 170 (2012), [arXiv:1210.2423](#).
- [36] G. V. Dunne and M. Ünsal, “New Nonperturbative Methods in Quantum Field Theory: From Large-N Orbifold Equivalence to Bions and Resurgence,” *Ann. Rev. Nucl. Part. Sci.* 66, 245 (2016), [arXiv:1601.03414](#).
- [37] J. Écalle, *Fonctions Resurgentes*, Publ. Math. Orsay 81, Université de Paris–Sud, Département de Mathématique, Orsay, (1981).
- [38] A. Erdélyi, *Higher Transcendental Functions*, The Bateman Manuscript Project, vol 1., New York–London (1953), <https://authors.library.caltech.edu/43491/>
- [39] Fokas, Athanassios S.; Its, Alexander R.; Kapaev, Andrei A.; Novokshenov, Victor Yu. *Painlevé transcedents: The Riemann–Hilbert approach*, *Mathematical Surveys and Monographs*, 128, Providence, R.I.: American Mathematical Society, (2006).
- [40] M. E. Fisher, “Critical Point Phenomena - the role of series expansions”, *Rocky Mount. J. Math.* 4, 181-201 (1974).
- [41] W. Florkowski, M. P. Heller and M. Spalinski, “New theories of relativistic hydrodynamics in the LHC era,” *Rept. Prog. Phys.* 81, no.4, 046001 (2018), [arXiv:1707.02282](#).

- [42] D. Gaiotto, G. W. Moore and A. Neitzke, “Wall-crossing, Hitchin Systems, and the WKB Approximation,” *Adv. Math.* **234**, 239-403 (2013), [arXiv:0907.3987](#).
- [43] S. Garoufalidis, A. Its, A. Kapaev and M. Marino, “Asymptotics of the instantons of Painlevé I,” *Int. Math. Res. Not.* **2012**, no. 3, 561 (2012), [arXiv:1002.3634](#).
- [44] D. S. Gaunt and A. J. Guttmann, “Asymptotic Analysis of Coefficients”, in *Phase Transitions and Critical Phenomena, Vol. 3*, C. Domb and M. S. Green (Eds) (Academic Press, 1974).
- [45] A. Gopal, L. N. Trefethen, “Representation of conformal maps by rational functions”, *Numer. Math.* **142**, 359-382 (2019), [arXiv:1804.08127](#).
- [46] E. G. Grassmann and J. Rokne, An explicit calculation of some sets of minimal capacity, *SIAM J. Math. Anal.* **6**, 242-249 (1975).
- [47] S. Gukov, M. Mariño and P. Putrov, “Resurgence in complex Chern-Simons theory,” [arXiv:1605.07615](#).
- [48] J. A. Hempel, On the uniformization of the n -punctured sphere, *Bull. London Math. Soc.* **20**, 97-115 (1980).
- [49] See A. V. Kitaev, “Elliptic asymptotics of the first and the second Painlevé transcendents”, *Uspekhi Mat. Nauk*, 49:1(295) (1994), 77–140; *Russian Math. Surveys*, 49:1 (1994), 81–150, and references therein.
- [50] H. Kober, *Dictionary of Conformal Representations*, Dover (1957).
- [51] M. Kontsevich, Y. Soibelman, Airy structures and symplectic geometry of topological recursion, [arXiv:1701.09137](#).
- [52] G.V. Kuz'mina, Estimates for the transfinite diameter of a family of continua and covering theorems for univalent functions, *Proc. Steklov Inst. Math.* **94**, 53-74 (1969).
- [53] N. S. Landkof, *Foundations of modern potential theory*, Springer-Verlag, New York–Heidelberg (1972).
- [54] D. S. Lubinsky, Rogers-Ramanujan and the Baker-Gammel-Wills (Padé) conjecture, *Annals of Mathematics*, 157, 847–889 (2003).
- [55] M. Mariño, “Nonperturbative effects and nonperturbative definitions in matrix models and topological strings,” *JHEP* **0812**, 114 (2008), [arXiv:0805.3033](#).
- [56] Frédéric Menous. Les bonnes moyennes uniformisantes et une application à la resommation réelle. *Annales de la Faculté des sciences de Toulouse : Mathématiques*, 6e série, 8(4):579–628, (1999).
- [57] A. Martinez-Finkelshtein, E. A. Rakhmanov, S. P. Suetin, Heine, Hilbert, Pade, Riemann, and Stieltjes: John Nuttall’s work 25 years later, *Contemporary Mathematics* 578, 165–193 (2012).
- [58] D. Masoero, “Poles of Integrale Tritronquee and Anharmonic Oscillators. Asymptotic localization from WKB analysis,” *Nonlinearity* **23**, 2501 (2010), [arXiv:1002.1042](#); “Poles of Integrale Tritronquee and Anharmonic Oscillators. A WKB Approach”, *J. Phys. A: Math. Theor.* 43 095201 (2010), [arXiv:0909.5537](#).

- [59] Z. Nehari, *Conformal Mapping*, Dover (1952).
- [60] V. Yu. Novokshenov, “Poles of Tricontroué Solution to the Painlevé I Equation and Cubic Anharmonic Oscillator”, *Reg. Chaotic Dyn.* **15**, 390 - 403 (2010).
- [61] C. Mitschi, D. Sauzin, *Divergent Series, Summability and Resurgence I, II*, Springer (2016).
- [62] initiated by F. Bornemann, P. Clarkson, P. Deift, A. Edelman, A. Its, and D. Lozier, <https://math.nist.gov/DLozier/PainleveProject/>
- [63] Ch. Pommerenke, *Boundary Behavior of Conformal Maps*, Springer-Verlag (1992).
- [64] J.-P. Ramis, J. Sauloy, C. Zhang, Local analytic classification of q-difference equations, [arXiv:0903.0853](https://arxiv.org/abs/0903.0853), *Astérisque* Volume: 355, (2013).
- [65] T. Ransford, *Potential theory in the complex plane*, vol. 28 of London Mathematical Society Student Texts, Cambridge University Press, Cambridge (1995).
- [66] R. Rossi, T. Ohgoe, K. Van Houcke and F. Werner, “Resummation of diagrammatic series with zero convergence radius for strongly correlated fermions,” *Phys. Rev. Lett.* **121**, no. 13, 130405 (2018), [arXiv:1802.07717](https://arxiv.org/abs/1802.07717).
- [67] E. B. Saff, *Logarithmic Potential Theory with Applications to Approximation Theory*, [arXiv:1010.3760](https://arxiv.org/abs/1010.3760) (2010)
- [68] W. Schlag, *A Course in Complex Analysis and Riemann Surfaces*, American Mathematical Society, Graduate Studies in Mathematics, vol. 154 (2014).
- [69] M. Serone, G. Spada and G. Villadoro, “ $\lambda\phi_2^4$ theory II. The broken phase beyond NNNN(NNNN)LO,” *JHEP* **1905**, 047 (2019), [arXiv:1901.05023](https://arxiv.org/abs/1901.05023).
- [70] H. Stahl, The Convergence of Padé Approximants to Functions with Branch Points, *Journal of Approximation Theory* **91**, 139–204 (1997).
- [71] M. A. Stephanov, “QCD critical point and complex chemical potential singularities,” *Phys. Rev. D* **73**, 094508 (2006), [arXiv:hep-lat/0603014](https://arxiv.org/abs/hep-lat/0603014).
- [72] G. Szegő, *Orthogonal Polynomials*, (American Mathematical Society, 1939); U. Grenander and G. Szegő, *Toeplitz forms and their applications*, (Univ. California Press, Berkeley, 1958).
- [73] H. S. Wall, General Theorems on the Convergence of Sequences of Pade Approximants, *TAMS*, Vol. 34, No. 2 (1932).
- [74] J. Zinn-Justin, *Quantum Field Theory and Critical Phenomena*, *Int. Ser. Monogr. Phys.* **113**, 1 (2002).
- [75] J. Zinn-Justin and U. D. Jentschura, “Multi-instantons and exact results I: Conjectures, WKB expansions, and instanton interactions,” *Annals Phys.* **313**, 197 (2004), [arXiv:quant-ph/0501136](https://arxiv.org/abs/quant-ph/0501136); “Multi-instantons and exact results II: Specific cases, higher-order effects, and numerical calculations,” *Annals Phys.* **313**, 269 (2004), [arXiv:quant-ph/0501137](https://arxiv.org/abs/quant-ph/0501137).